HHS Public Access

Author manuscript

ACS Nano. Author manuscript; available in PMC 2018 February 28.

Published in final edited form as:

ACS Nano. 2017 February 28; 11(2): 1869–1883. doi:10.1021/acsnano.6b07895.

Pro-Inflammatory and Pro-Fibrogenic Effects of Ionic and Particulate Arsenide and Indium-Containing Semiconductor Materials in the Murine Lung

Wen Jiang[†], **Xiang Wang**[†], **Olivia J. Osborne**[†], **Yingjie Du**[†], **Chong Hyun Chang**[†], **Yu-Pei Liao**[‡], **Bingbing Sun**[†], **Jinhong Jiang**[†], **Zhaoxia Ji**[†], **Ruibin Li**[†,§], **Xiangsheng liu**[‡], **Jianqin Lu**[‡], **Sijie Lin**[†,◊], **Huan Meng**[‡], **Tian Xia**[†,‡], and **André E. Nel**[†,‡,*]

[†]Center for Environmental Implications of Nanotechnology, California NanoSystems Institute, University of California Los Angeles, 570 Westwood Plaza, Los Angeles, CA 90095, United States

[‡]Division of NanoMedicine, Department of Medicine, University of California Los Angeles, 10833 Le Conte Ave, Los Angeles, CA 90095, United States

[◊]College of Environmental Science and Engineering State Key Laboratory of Pollution Control and Resource Reuse, Tongji University, Shanghai, China, 200092

[§]School of Radiation Medicine and Protection & School for Radiological and Interdisciplinary Sciences (RAD-X), Medical College of Soochow University, Suzhou, Jiangsu 215123, China

Abstract

We have recently shown that the toxicological potential of GaAs and InAs particulates in cells is size- and dissolution-dependent, tending to be more pronounced for nano- *vs.* micron-sized particles. Whether the size-dependent dissolution and shedding of ionic III-V materials also apply to pulmonary exposure is unclear. While has been demonstrated that micron-sized III-V particles, such as GaAs and InAs, are capable of inducing hazardous pulmonary effects in an occupational setting, as well as in animal studies, the effect of sub-micron particles (*e.g.*, the removal of asperities during processing of semiconductor wafers) is unclear. We used cytokine profiling to compare the pro-inflammatory effects of micron- and nanoscale GaAs and InAs particulates in cells as well as the murine lung 40 h and 21 days after oropharyngeal aspiration. Use of cytokine array technology in macrophage and epithelial cell cultures demonstrated a proportionally higher increase in the levels of extracellular matrix metalloproteinase inducer (EMMPRIN), macrophage migration inhibitory factor (MIF), and interleukin 1β (IL-1β) by nano-sized (n) GaAs and n-InAs as well as As(III). n-GaAs and n-InAs also triggered higher neutrophil counts in the bronchoalveolar lavage fluid (BALF) of mice than micronscale particles 40 h post-aspiration, along with increased production of EMMPRIN and MIF. In contrast, in animals sacrificed 21 days

[*]Address correspondence to: André E. Nel, M.D./Ph.D., Department of Medicine, Division of NanoMedicine, UCLA School of Medicine, 52-175 CHS, 10833 Le Conte Ave, Los Angeles, CA 90095-1680, USA, Tel: (310) 825-6620, Fax: (310) 206-8107, anel@mednet.ucla.edu.

Supporting Information Available: Detailed methods, characterization of III-V materials, Cytokine microarray study, total cell count in mice study, as well as structure determination of indium precipitates. This material is available free of charge *via* the Internet at http://pubs.acs.org.

after exposure, only n-InAs induced fibrotic lung changes as determined by increased lung collagen as well as increased levels of TGF-β1 and PDGF-AA in the BALF. A similar trend was seen for EMMPRIN and matrix metallopeptidase (MMP-9) levels in the BALF. Nano- and micron-GaAs had negligible sub-acute effects. Importantly, the difference between the 40 h and 21 days data appears to be biopersistence of n-InAs, as demonstrated by ICP-OES analysis of lung tissue. Interestingly, an ionic form of In, $InCl_3$, also showed pro-fibrogenic effects due to the formation of insoluble $In(OH)_3$ nanostructures. All considered, these data indicate that while nanoscale particles exhibit increased pro-inflammatory effects in the lung, most effects are transient, except for n-InAs and insoluble $InCl_3$ species that are biopersistent and trigger pro-fibrotic effects. These results are of potential importance for the understanding the occupational health effects of III-V particulates.

Keywords

III-V materials; size; occupational disease; pro-inflammatory cytokine; lung inflammation; lung fibrosis

---

III-V semiconductor materials, including GaAs and InAs, are widely used for device applications such as light-emitting diodes (LEDs), lasers, detectors in communication devices, biosensors and bio-imaging.[1, 2] Manufacturing of these materials makes frequent use of abrasive techniques such as chemical-mechanical planarization (CMP) of semiconductor wafers to prepare the material surface for further processing. CMP relies on the use of engineered nanomaterials (ENMs) such as SiO_2, CeO_2 and Al_2O_3 in primary slurries to remove asperities from the wafer surface.[3] These include the release of III-V materials, which together with other noxious chemical substances may contribute to the formation of even more hazardous spent slurries.[3, 4] Both the primary and spent slurry materials could exert adverse health effects to semiconductor workers, including the potential of pulmonary hazard due to exposure to aerosolized emissions.[3, 5, 6] While occupational studies have suggested that the nanoparticles (NPs) contained in primary slurries for the performance of CMP can become aerosolized, leading to inhalation exposure, the collection of filter samples and direct-reading instruments for detecting metal oxides indicate that the particle counts can be kept low in a well-controlled working environments in the semiconductor industry.[7] However, there are no contemporary data about the presence and concentration of III-V particulates or fragments which may attach to or be co-mixed with primary particles in aerosolized materials released in the semiconductor workspace.[8] This is important from the perspective of the large workforce in the industry as well as evidence that micronscale GaAs particulates can induce pro-inflammatory effects in the lung,[9, 10] while InAs and $InCl_3$ may induce fibrotic changes and restrictive pulmonary function abnormalities.[11, 12]

We have recently shown that commercially acquired GaAs and InAs particulates can exert size and dissolution-dependent toxicity in macrophages and epithelial cells.[13] Interestingly, nanoscale III-V particles were more toxic than micron-sized particles.[13] However, while it is known that micron-sized III-V particulates can lead to *in vivo* toxicological changes, no experimental *in vivo* studies have been undertaken to assess the toxicity of nano-sized

particulates. For instance, in a 2-year inhalation study in rats performed by the National Toxicology Program (2000), it was demonstrated that micron-sized GaAs particles can result in inflammatory and proliferative changes in the respiratory tract, with occasional appearance of lung tumors in female rats.[14] Moreover, the US Environmental Protection Agency (EPA) classified GaAs as an immunotoxicant based on the As and Ga release,[15] in addition to the demonstration that GaAs particles can induce dose- and time-dependent suppression of the immune system after intratracheal administration in mice.[16] A study by Webb *et al.* demonstrated that the As release from dissolving micronscale GaAs particulates can lead to pulmonary fibrosis.[17–19] A two-year study of InAs toxicity in the golden hamster found that micron-sized InAs induced more severe pulmonary lesions and higher serum indium levels than InP due to differences in particle dissolution.[20] Tanaka *et al.* reported that micron-sized InAs particles induced more severe pulmonary effects in golden hamsters than GaAs and As_2O_3, while Blazka *et al.* demonstrated acute inflammatory and fibrotic lung changes in response to ionic $InCl_3$.[13, 21, 22] In contrast, the impact of GaAs and InAs exposure in humans is much less clear. Luo *et al.* found that male Taiwanese fabrication workers employed in process-, maintenance- and equipment engineering had an increased prevalence of restrictive pulmonary function abnormalities and decreased white blood cell counts compared to non-fabrication workers.[23, 24] A study in Scotland also found that female workers in the semiconductor industry showed an increased incidence of lung cancer and increased mortality compared to normal population.[25] However, the sample size was limited and the study also stated that more investigation is required to confirm the significance of the findings.[6, 26]

We have previously demonstrated that there is a significant tendency for nanoscale metal oxides to exert increased pulmonary impacts compared to micronscale particulates, based on size and nanoscale biophysicochemical interactions that could lead to triggering of adverse outcome pathways in the lung.[27, 28] Considering the knowledge gap about the impact of micron- *vs.* nanoscale III-V particulates, as well as the hazard potential of ionic III-V species that may be released from the particles, we engaged in a systematic examination of acute and sub-acute pulmonary effects of commercially acquired III-V materials. Utilizing cytokine profiling in epithelial cells and macrophages as guidance, this discovery was used for conducting oropharyngeal aspiration studies in mice to determine if selected micronscale, nanoscale and ionic III-V materials exert pro-inflammatory effects in the murine lung, 40 h and 21 D after oropharyngeal instillation. The results indicate that while both n-GaAs and n-InAs induce transient pro-inflammatory in the lung, n-InAs and insoluble $InCl_3$ induced fibrotic changes, which could be related to increased biopersistence after 21 D. These results are important in considering to what extent monitoring of sub-micron III-V particulates and ionic species should be considered for assessing the occupational hazards of related materials in the workplace.

RESULTS

Physicochemical Characterization and Cytotoxicity Profiling of III-V Materials

The physicochemical properties of micron- (m-) and nano-sized (n-) III-V arsenides under *in vitro* and *in vivo* conditions were determined in water and cell culture media (RPMI and

BEGM), as well as *in vitro* simulated bronchoalveolar lavage fluid (sBALF) and simulated interstitial lung fluid (Gamble's solution). Particle size (Table 1) and zeta potential (Table 2) were determined by the use of dynamic light scattering (DLS) and a zeta potential analyzer, respectively. Transmission electron microscopy (TEM) images showed that m-GaAs and m-InAs core sizes ranged from 100 to 800 nm, while nano-sized particles were <100 nm in size (Figure 1). Also, the micron-sized particles had larger hydrodynamic diameters than the nanoscale particles in all media, with the trend being most pronounced in PBS and Gamble's solution, where the hydrodynamic diameter was >1 μm (Table 1). Nanoscale particles have the tendency to aggregate, yielding a hydrodynamic size range of 200–600 nm. All the particles showed negative zeta-potentials in the media tested (Table 2).

Since our goal is to study the pulmonary effects of III-V materials, two representative cell lines, a differentiated macrophage (THP-1) and a human bronchial epithelial cell line (BEAS-2B), were used to perform cytotoxicity studies over a 24 h period. Both cell death as well as viability studies were performed using a molar weight metric to compare the particles to ionic III-V materials, as shown in Table 3. We found n-GaAs had similar toxicity as As(III), capable of inducing the highest rate of cell death (~ 65%) at 0.7 μmol/mL (100 mg/mL) (Figure 2A). By comparison, the cell death rate was ~ 50% for As(V) and 30% for m-GaAs. Both InAs particulate sizes, $GaCl_3$ and $InCl_3$ exerted little toxicity in THP-1 cells at 24 h. The assessment of cellular viability, as reflected by ATP levels, showed the same outcome as the CellTox assay, where n-GaAs and As(III) induced the highest cytotoxicity at 24 h (Figure 2B). BEAS-2B cells showed similar cytotoxicity and viability results as THP-1 cells (Figure S1).

Since it is known that III-V arsenides induce oxidative stress,[29] we measured cellular glutathione (GSH) levels with a luminescence-based GSH-Glo assay. This demonstrated that exposure of THP-1 cells to 0.35 μmol/mL n-GaAs could induce a significant decrease in cellular GSH levels compared to m-GaAs (Figure 2C). There was also a significant decrease in luminescence activity in response to As(III) and As(V), as well as Co_3O_4 NPs (used as a positive control). In contrast, both InAs particulate sizes, $GaCl_3$ and $InCl_3$ had little effect on GSH levels in THP-1 cells. The same trend was seen in BEAS-2B cells, with n-GaAs, As(III) and As(V) inducing the most noticeable decreases in GSH (Figure S1C). We have previously demonstrated that 85% and 15% of the As released from GaAs is in the form of As(III) and As(V), respectively.[13] All considered, these data indicate that the arsenic moiety in GaAs induces cellular oxidative stress as one of the mechanisms contributing to an adverse cellular outcome.

In vitro Pro-inflammatory Effects of III-V Materials in THP-1 Cells

According to the hierarchical oxidative stress response paradigm for pro-oxidative materials, moderate levels of ROS production, are capable of inducing pathways that lead to the production of pro-inflammatory cytokines.[30] In order to screen for cytokines that may be induced by III-V materials, we use a commercial cytokine array, Proteome Profiler™ Human XL Cytokine Array Kit, to analyze 102 individual cytokines and proteins (Table S1) released from THP-1 cells during treatment with micron- and nanoscale GaAs at 0.043 and 0.173 μmol/mL. As(V) was used as a comparative control. Among 102 possible cytokines,

THP-1 cells produced 18 of these (Table 4 and Figure S2A). ImageJ analysis was used to assess the pixel density of the array films, as shown in the example in Figure S2A–B. While n-GaAs either had no or down-regulatory effects on cytokine production (Figure S2B), the relative abundance of (i) extracellular matrix metalloproteinase inducer (EMMPRIN) and (ii) macrophage migration inhibitory factor (MIF) were increased at n-GaAs concentrations of 0.043 and 0.173 μmol/mL (Table 4, Figure S2C). m-GaAs had a lesser effect while As(V) was comparable to n-GaAs (Figure S2C).

EMMPRIN and MIF play important roles in the recruitment of lymphocytes and granulocytes to the inflamed tissue.[31, 32] To validate the cytokine array data, ELISA assays for EMMPRIN and MIF were used to assess the effect of particle size in THP-1 cells (Figure 3). n-GaAs and n-InAs induced a significantly greater increase in EMMPRIN levels than micron-sized particles at doses of 0.174 and 0.7 μmol/mL (Figure 3A). This was comparable to the effect of As(III) (Figure 3A). The ionic forms Ga, In and As(V) also induced dose-dependent increases of EMMPRIN but not as high as As(III). Positive control ZnO NPs triggered the highest EMMPRIN response at 0.7 μmol/mL. n-GaAs and n-InAs induced a higher MIF responses than m-GaAs and m-InAs, respectively, with n-GaAs approximating the effect of As(III) (Figure 3B). These results indicate that the arsenic moiety, particularly As(III), released from n-GaAs and n-InAs induce EMMPRIN and MIF production in THP-1 cells.

III-V Particles and Ionic Forms Induce Acute Pulmonary Inflammation

To determine if the *in vitro* pro-inflammatory effects of III-V materials predict *in vivo* response outcomes, we used oropharyngeal aspiration in C57BL/6 mice, which were sacrificed after 40 h. The calculated dose for the study was based on cleanroom airborne exposure levels for As in factory workers, as shown in Table 5. To date, only As concentrations have been monitored to reflect the exposure of GaAs because no analytical methods are available to reliably assess aerosolized GaAs compounds.[33] Moreover, As is generally considered as the most toxic III-V element and its occupational exposure limits have been established for global use, while the analytical methods to determine the Ga and In are very limited.[33] Based on a frequently cited historical report by Sheehy *et al.* in 1993, who detected aerosolized As concentrations as high as 2.7 mg/m^3 in a factory producing optoelectronic devices and integrated circuits,[34] we calculated a GaAs exposure level of 5.2 mg/m^3. This likely represents a worst case scenario that is based on a high minute ventilation, high rate of deposition, and absence of clearance. An exposure level of 5.2 mg/m^3 translates into a weekly exposure dose of 74.88 mg GaAs (8 h/day, 5 days/week) in this hypothetical situation, assuming a ventilation rate of 20 L/min and a NP deposition fraction of 30% in a healthy human subject. When converted to surface area dose based on a human alveolar surface area of 102 m^2, this translates to a deposition level of 734.12 $\mu g/m^2$. This is equivalent to a one-time murine exposure dose of 1.468 mg/kg per mouse, assuming an alveolar surface area of 0.05 m^2 in a 25 g mouse. Consequently, we chose an installation dose of 0.014 mmol/kg for each of the III-V materials (equal to 1–4 mg/kg based on the molar weight in Table 3) to perform pulmonary aspiration in mice. ZnO NPs were used at the same molar dose as a positive control and induced a robust neutrophilic collection and cytokine responses in the BALF after 40 h (Figures 4 and S3). Most of the particulate and

ionic III-V materials also induced neutrophilic inflammation in the lung, with $GaCl_3$ and $InCl_3$ inducing the highest levels, followed by n-InAs (Figure 4A). These responses were significantly higher than m-InAs, both forms of GaAs, As(III) and As(V). n-GaAs and n-InAs induced higher levels of EMMPRIN, matrix metallopeptidase (MMP-9) and lipopolysaccharide-inducible CXC chemokine (LIX) in the BALF than micronscale particles (Figure 4B-4D). However, for MIF, all particles, $InCl_3$ and As ions induced approximately the same level of increase except for $GaCl_3$ (Figure 4E). These cytokines play important roles in monocyte and neutrophil recruitment to the lung.[35–37] LIX, has the same role as IL-8 in humans. It is interesting, therefore, that all nano-sized III-V particulates induce dose-dependent increases in IL-8 production in human-derived THP-1 cells (Figure S4). The presence of mild inflammatory changes in the lung was confirmed by H&E staining (Figure S5). While n-GaAs, n-InAs, As(III) and ZnO NPs induced focal cellular infiltration in the area of alveoli and blood vessels, along with alveolar membrane thickening, micron-sized particles as well as ionic Ga, In and As(V) had no noticeable effect.

The acute pro-inflammatory changes were compared to elemental analysis of the lung tissue, using ICP-OES analysis (Figure 4F). This demonstrated that nanoscale GaAs and InAs led to comparable increases in the As content in the lung, while micronscale particles had lesser effects. This likely reflects higher retention of the nanoscale compared to the micron scale III-V particles as a result of the lower clearance of nanoscale particles by macrophages *in vivo*.[38–40] The same trend was found for Ga and In levels in the lung, with nanoscale particles inducing bigger increases. No lung deposition was seen during aspiration of ionic forms of As and Ga. In order to confirm the role of NPs dissolution in pulmonary accumulation, dissolution studies were performed in s simulated BALF (sBALF) and Gamble's solution (Figure S6). Highly soluble GaAs of both size ranges showed a dramatic increase in dissolution in sBALF over 24 and 40 h compared to InAs. The dissolution of n-GaAs led to the dissolution of 40% As and 15% Ga after 40 h, which is twice the level of As shedding and 1.5 times that of Ga from m-GaAs (Figure S6A). To the contrary, InAs in both sizes resulted in <5% As and negligible In release from the particles. Dissolution in Gamble's solution, which is representative of interstitial lung fluid, showed the same trend as in sBALF, except that n-GaAs sheds up to 50% As and 30% Ga at 40 h. Even though the higher As release from n-GaAs *vs*. n-InAs is correlated to more robust *in vitro* effect*s* (Figure 2), the same materials had comparable acute pulmonary effect at 40 h (Figure 4A-4E), possibly due to more rapid clearance of n-GaAs from the lung (Figure 4F).

n-InAs and $InCl_3$ but not GaAs Induce Sub-Acute Pulmonary Fibrosis in Mice

InAs and indium compounds have been reported to induce chronic damage in the hamster lung.[11, 12] Since we have determined for a number of biopersistent nanomaterials (*e.g.*, carbon nanotubes, rare earth oxides) that IL-1β production and downstream triggering of pro-fibrotic growth factor production can lead to fibrotic changes in the lung,[41–43] IL-1β release by III-V materials were assessed *in vitro* and *in vivo*. Cellular studies, using differentiated THP-1 cells, demonstrated a dose-dependent increase in IL-1β production by all III-V particulates and ionic materials (Figure 5). Monosodium urate (MSU) was used as a positive control. These effects were most prominent at a dose more than 0.174 μmol/mL, where nanoscale particles had a stronger effect than micronscale particles. Subsequent

pharyngeal aspiration in C57BL/6 mice, using the same dosimetry as in the acute study (Table 3), allowed us to assess pro-fibrotic effects in the lung. Alpha-quartz (Min-U-Sil, MUS) was used as a positive control that produces a strong pro-fibrogenic effect at 21 D after initial pharyngeal aspiration of 5 mg/kg.[44] BALF cell counts in the animals, euthanized after 21 D, demonstrated that n-InAs has the most robust effect for increasing infiltration of eosinophils, neutrophils and lymphocytes, followed by $InCl_3$, m-InAs and MUS (Figure 6A). In contrast, IL-1β production occurs earlier and cytokine levels do not remain elevated for 21 D (Figure S7). There was a significant response to n-InAs and $InCl_3$ in the production of the pro-fibrogenic growth factors, PDGF-AA and TGF-β1 (Figure 6B and 6C). In contrast, there were lesser or no responses to m-InAs, GaAs, As(III) and As(V). Moreover, we also observed higher EMMPRIN and MMP-9 levels for n-InAs and $InCl_3$ with smaller effects for m-InAs and little or no effect for GaAs (Figure 6D and 6E).

Histological examination, using Masson's trichrome staining, showed prominent fibrotic changes in the lung in response to n-InAs and MUS, while m-InAs and $InCl_3$ induced milder effects (Figure 7A). Moreover, biochemical quantification of the collagen content in the lung showed a good agreement with trichrome staining, with n-InAs, m-InAs, $InCl_3$ and MUS inducing significant increases in collagen as determined by the Sircol assay (Figure 7B). Additionally, ICP-OES analysis of the elemental content of the lungs after 21 D showed results that are consistent with the pro-fibrogenic changes, namely higher levels for As and In during exposure to n-InAs, compared to m-InAs or n-GaAs (Figure 7C). While In could be detected in the lung following exposure to $InCl_3$, it was not as high as n-InAs. These data seem to indicate that the biopersistence of In (and perhaps As) during n-InAs exposure as well as $InCl_3$ precipitation (Figure S8) in the lung plays a role in triggering of pro-fibrotic responses that do not occur for GaAs.

DISCUSSION

We conducted *in vitro* and *in vivo* studies to understand whether nanoscale III-V particulates and ionic species pose a hazard to the lung during acute and sub-acute exposure. *In vitro* protein array data and ELISA measurements demonstrated that nanoscale GaAs and InAs particles induce a series of cytokines (EMMPRIN, MIF, IL-8 and IL-1β) that were elevated to the same degree during exposure to micronscale particulates. The *in vitro* cytokine profile was consistent with the generation of more prominent neutrophilic inflammation in the lung 40 h after the aspiration of n-GaAs, n-InAs, $GaCl_3$ and $InCl_3$, which also induced higher production of LIX, EMMPRIN, and MIF in the BALF. In contrast, assessment of the pulmonary hazard 21 D after oropharyngeal instillation demonstrated that n-InAs and $InCl_3$ induced fibrotic changes accompanied by pro-fibrogenic factors such as TGF-β1 and PDGF-AA. No fibrotic effects were seen with all sizes of GaAs. The sub- acute effects of n-InAs could be ascribed to biopersistence, as demonstrated by ICP-OES analysis of lung tissue. This analysis also demonstrated that $InCl_3$ leads to the formation of insoluble, biopersistent precipitates that are harmful. Collectively, these data indicate that, dependent on size and composition, specific III-V particulates and ionic species do have the potential to induce acute and sub-acute pulmonary effects that can be related to the cytokine profile and biopersistence of the materials.

The key finding in this study was the importance of particle size in generating harmful pulmonary effects by III-V materials, with nanoscale particulates being more harmful than micronscale particles *in vivo*. Particle size is important for dissolution and release of ionic III-V species as well as clearance from the lung (Figure 4F, Figure 7C). The slow clearance of nanoscale III-V particles could be related to slow uptake and removal by pulmonary macrophages,[38-40] while the dissolution of n-GaAs leads to rapid release of As(III) and As(V). In contrast, n-InAs is less soluble (Figure S6) and leads to biopersistence (Figure 7C). Consequently, there are significant differences between n-GaAs and n-InAs in terms of their impact on the lung. While the rapid release of As(III) and As(V) by n-GaAs induces oxidative stress and the production of a specific set of cytokines that contribute to acute pro-inflammatory changes in the lung, the slower and incomplete (<5%) n-InAs dissolution leads to pro-fibrogenic effects that are not seen with GaAs (Figures 6). Moreover, the biopersistent InAs NPs may be taken up into the acidic lysosomal compartment in macrophages, where a faster initial rate of dissolution could lead to the In release and the formation of insoluble $In(OH)_3$ precipitates, which are biopersistent and capable of driving pro-fibrogenic responses (Figure 7, Figure S8). This effect is mimicked by $InCl_3$ precipitates formed in sBALF. In addition to triggering the release of LIX, EMMPRIN and MMP-9, In precipitates are capable of inducing IL-1β production, which could explain the fibrotic changes in the lung (Figure S8C–S8F).

Another important finding is the elucidation of EMMPRIN, MIF and MMP-9 as potential biomarkers for the adverse pulmonary effects of III-V arsenide materials. These cytokines were picked up during cellular screening by cytokine array technology and differ from the cytokines that typically contribute to the toxicological effect of metal oxide NPs.[27, 28] Interestingly, EMMPRIN, MIF and MMP-9 were produced during the acute as well as sub-acute pulmonary responses (Figure 4 and Figure 6). EMMPRIN and MIF production requires transcriptional activation of the respective genes by the NF-κB cascade.[45, 46] In this regard, it is known that arsenic-induced toxicity involves NF-κB activity *in vitro*,[47–49] as well as in arsenic-exposed human subjects.[50] Thus, As release from III-V arsenides (Figure S6) could induce EMMPRIN and MIF production through the activation of the NF-κB cascade. EMMPRIN is a transmembrane glycoprotein belonging to the immunoglobulin superfamily, and plays an important role in the recruitment of immune cells to sites of inflammation.[31, 51] EMMPRIN is up-regulated in a number of human inflammatory diseases, where it plays a role in enhancing the invasiveness of monocytoid cells, in addition to inducing the synthesis of MMPs in adjacent fibroblasts.[52] EMMPRIN is involved in both acute and chronic lung inflammation.[51–53] This includes the demonstration of spontaneously enhanced EMMPRIN production in the macrophages of patients with lung fibrosis.[53] MIF is a multifunctional cytokine that can trigger the production of a cascade of downstream cytokines and mediators, including IL-1β and IL-8.[32, 54] The upregulation of MIF plays an important role in lung injury, fibrosis and cancer.[36, 55–58] MIF production can be triggered by ROS,[8, 32] and it promotes the generation of MMPs.[59–61] The MMPs are a diverse family of extracellular proteinases, which are known to be involved in various inflammatory disease processes, tissue remodeling and healing process.[62] Among them, MMP-9 plays an important role at different stages of lung injury and repair of the alveolar epithelium.[62, 63] MMP-9 is mainly released by neutrophils.[37, 62, 64] but it could be produced by fibroblasts in

response to EMMPRIN stimulation.[52] It is responsible for neutrophil transmigration,[37] degradation of extracellular matrix components, as well as TGF-β mediated collagen deposition and airway remodeling.[63] Collectively, the III-V arsenides may induce pulmonary effects by releasing arsenic ions to induce NF-κB activation and further promote EMMPRIN, MIF production, which activate MMP-9 generation to induce lung inflammation and fibrosis. The consistent association of EMMPRIN, MIF and MMP-9 to the toxicological effects of III-V arsenides (Figure 3, Figure 4 and Figure 6) introduces possible biomarkers that can be used to track adverse pulmonary responses to III-V materials, and could also serve as targets for anti-inflammatory therapy.[51, 65] However, further studies are required to confirm the molecular mechanisms and production of these proinflammatory products in humans during occupational exposure.

What relevance, if any, do these findings have for the assessment and control of the potential hazards from the aerosolized release of particulates in the semiconductor industry? There is evidence that the use of SiO_2, CeO_2, and Al_2O_3 NPs during CMP can be detected by direct readout and on filter samples retrieved from the wastewater treatment area in semiconductor facilities.[7, 66, 67] However, little is known about the presence and amounts of aerosolized III-V fragments. While the analysis of spent CMP slurries clearly demonstrate the presence of micron and submicron scale III-V particulates on the surface of pristine particle components,[68] not much is known about actual III-V airborne exposure levels in contemporary manufacturing facilities. Until now, the concentration of toxic As served as the metric for tracking occupational exposures to III-V arsenides because no analytical methods are available for other III-V compounds.[33] The recommended exposure limit (REL) of As (0.002 mg/m^3 every 15 minutes) as well as In (time-weighted average 0.1 mg/m^3) from the National Institute for Occupational Safety and Health (NIOSH) are designed for elemental As and In, but not for aerosolized III-V particles. Additionally, no occupational exposure limits have been set for Ga. Because of the limitations of the current technology to characterize aerosolized NPs, no RELs have been established for III-V NPs, and there are no contemporary reports for assessing III-V particulate concentrations in the semiconductor industry. However, in a comprehensive review of As levels in the semiconductor manufacturing industry, Park *et al.* have documented an exposure level as high as 218.6 $\mu g/m^3$ among 423 airborne As measurements.[69] This is approximately 10 fold lower than the historical data (2.7 mg/m^3) that we have used for our animal dosimetry calculations (Table 5) and may reflect improvement in engineering and environmental control processes since 1993.[34] The *in vivo* dosimetry based on the report in 1993 is comparable to *in vitro* study through normalizing the surface area dose in the murine airways compared to the normalized surface area dose of particles in the tissue culture dish. Accordingly, exposure to 2 mg/kg GaAs is equivalent to a surface area dose of 1 mg/m^2 in the mouse lung. Assuming that 1 mg/m^2 of GaAs *in vitro* is homogeneously distributed in the tissue culture dish, covered by a cellular layer 10 μm deep, the cellular surface area dose would be 100 μg/mL. Thus, our *in vitro* dose range of 6.25–100 μg/mL is in the ballpark of the *in vivo* dose. It is also possible to establish the *in vitro* exposure dose based on using the *in vitro* Sedimentation, Diffusion and Dosimetry (ISDD) model.[70] The *in vivo* high dose used in this study represents a worst case scenario from an occupational perspective. In contrast to the response to the bolus dose, the exposure to lower doses may not reach a threshold toxicological effect; however,

repeated or chronic low dose exposures could lead to a sufficient lung burden due to changes in the rates of dissolution or lung clearance to result in biopersistence and toxicity. For logistical reasons it was not possible to explore this consideration in the current studies, but have previously shown how this type of scenario could be studied by comparing bolus *vs.* repetitive dose administration of fumed silica in the lung.[71] It is also important to consider that the release of arsenic from III-V arsenides at chronic low exposures might induce lung cancer.[14, 71] In spite of using what may currently constitute an unrealistic high-dose in our studies, it is important to be aware of dosimetry considerations when assessing exposures to III-V particulates in the semiconductor industry, particularly in the maintenance areas. Successful technology has been implemented to assess the airborne spread of nanoparticles contained in the primary CMP slurries.[72, 73] Moreover, recent NIOSH guidelines called the necessity for improved identification and quantification of aerosols during the CMP process.[7]

CONCLUSION

We compared the pulmonary effects of nano- and micron-sized III-V materials *in vitro* and *in vivo*. Our study elucidates the critical role of particle size, dissolution and biopersistence in the potential of these materials to induce acute and sub-acute pulmonary effects in mice. We demonstrated that nanoscale GaAs and InAs are more prone to inducing adverse pulmonary effects than micronscale particles. While nanoscale GaAs and InAs particulates could induce acute pulmonary inflammation that was accompanied by the increase of EMMPRIN, MIF, and LIX levels in the lung, only n-InAs induced pro-fibrotic effects that were accompanied by the presence of TGF-β1, PDGF-AA, EMMPRIN and MMP-9 levels in the BALF. The transient effects of GaAs could be ascribed to rapid rate of dissolution and clearance from the lung, but the sub-acute effects of n-InAs are related to slow dissolution and biopersistence. These data demonstrate the importance of particle size, composition and biopersistence in the impact of respirable III-V materials in the lung.

MATERIALS AND METHODS

III-V Material Dispersion and Physicochemical Characterization

Micron-sized GaAs and InAs particles were purchased from American Elements (LA, CA, USA). Nano-sized GaAs and InAs were obtained from NN-lab (Fayetteville, AR, USA). All the particles were washed 3 times in DI water (resistivity>18Ωcm) and reconstituted as 10 mg/mL stock solutions by probe sonication for 1 min. The ionic forms, $GaCl_3$, $InCl_3$, $NaAsO_2$ (As^{III}) and $Na_2HAsO_4 \cdot 7H_2O$ (As^{V}) were purchased from Sigma-Aldrich. All the particles and ionic forms were prepared as 10 mg/mL stock solutions. The primary particle sizes and morphologies were determined by Transmission Electron Microscopy (TEM) in a JEOL 1200 EX microscope, with 80 kV accelerating voltage. DLS data and zeta potential were obtained using a ZetaPALS instrument (Brookhaven Instruments Corporation, Holtsville, NY). III-V stock solutions (10 mg/mL) were diluted to a final of 50 μg/mL in water, cell culture media, simulated bronchoalveolar lavage fluid (sBALF) or simulated interstitial lung fluid (Gamble's solution). THP-1 cells were cultured in Roswell Park Memorial Institute (RPMI) 1640 medium (Invitrogen, USA), supplemented with 10% FBS

(Gemini Bio-Products, West Sacramento, CA), while BEAS-2B cells were cultured in Bronchial Epithelial Growth Medium (BEGM) (Lonza, USA), supplemented with growth factors (SingleQuot Kit Suppl. & Growth Factors, Lonza) and 2 mg/mL bovine serum albumin (BSA). The sBALF was made from PBS, supplemented with 0.6 mg/mL BSA and 0.01 mg/mL dipalmitoylphosphatidylcholine (DPPC). Gamble's solution was reconstituted according to Marques' protocol, using 0.095 g/L $MgCl_2$, 6.019 g/L NaCl, 0.298 g/L KCl, 0.126 g/L Na_2HPO_4, 0.063 g/L Na_2SO_4, 0.368 g/L $CaCl_2 \cdot 2H_2O$, 0.574 NaOAc, 2.604 g/L $NaHCO_3$, as well as 0.097 g/L sodium citrate carbonate dissolved in DI water, with pH adjusting to 7.4.[74]

Assessment of III-V Cytotoxicity and Intracellular GSH Content

THP-1 and BEAS-2B cells were obtained from ATCC (Manassas, VA). Briefly, 3×10^4 THP-1 cells were pretreated with 1 μg/mL phorbol 12-myristate 13-acetate (PMA) in 0.1 mL RPMI 1640. BEAS-2B cells were cultured at 2×10^4 in 0.1 mL BEGM in each well. All the cells were plated at 37 °C in a humidified 5% CO_2 atmosphere overnight. The cell culture medium in each well was replaced by 100 μL of a media suspension, containing freshly made particulates, ionic forms, ZnO or MUS (Min-U-Sil, α-quartz) solution in either RPMI 1640 (THP-1) or in BEGM (BEAS-2B cells) at a final concentration range of 0.07–0.7 μmol/mL (Table 3). Cell death was determined by the CellTox™ Green Cytotoxicity Assay (Promega Corporation, Madison, WI, USA) in a Costar™ 96-well black-bottom plate. The CellTox™ Green fluorescence kit was diluted in Assay Buffer (1:500) and 100 μL added to each cell culture well for 1 h. The fluorescence intensity was read on a SpectraMax M5 microplate spectrophotometer at $485nm_{Ex}/525nm_{Em}$. The ATP content as a measure metric for cell viability was assessed by ATPlite 1step Assay (PerkinElmer, Boston, MA, United States) in white-bottom Costar™ 96-well plates. After incubation with III-V materials or the positive control for 24 h, the culture media were saved for the measurement of cytokines. The cells were incubated with 100 μL reconstituted ATPlite 1step reagent for 15 min. The luminescence intensity was read on a SpectraMax M5 microplate spectrophotometer. Cellular GSH content was determined by using a luminescence-based GSH-Glo assay (Promega, USA) at the dose of 0.35 μmol/mL. Luciferin-NT and Glutathione S-Transferase were diluted in the GSH-Glo™ Reaction Buffer at a ratio of 1:100 and incubated with cells for 30 min. Subsequently, reconstituted the Luciferin Detection Reagent was added for 15 min. The luminescence intensity was read in the same spectrophotometer.

Assessment of Cellular Cytokine Release by Microarray and ELISA Methods

The Proteome Profiler™ Human XL Cytokine Array Kit (Cat. No. ARY022, R&D System), comprised of pre-coated antibody arrays attached to a membrane, was used to profile 102 cytokines in the supernatant of THP-1 cells. The cells were prior exposed to micron-, nano-sized GaAs and As(V) at 0.043 and 0.173 μmol/mL for 24 h. Duplicate samples were used for each cytokine in the panel. The array membranes were blocked with 2 ml blocking buffer for 1 h. After decanting the blocking buffer, the membranes were overlaid with 1.5 mL of diluted supernatants and incubated overnight at 2–8 °C. The membranes were washed 3 times, followed by adding 1.5 mL of the diluted detection antibody for 1 h. After repeating the washing procedure, 2.0 mL Streptavidin-HRP was added to each well and incubated for

30 min. 1.0 mL Chemi Reagent Mix was added onto each membrane after washing and reacted for 1 min. The membranes were exposed to X-ray film for 2 min. The pixel density of each spot was determined using an Epson Perfection V500 Photo Scanner. The positive signals seen on the developed film is shown in Figure S2A. The average pixel density of the each pair of spots was determined by ImageJ 1.46r software, and compared to the pixel density on different arrays, according to which the relative change in each cytokine concentration could be determined. For ELISA analysis, THP-1 cells were exposed to III-V materials over the concentration range 0.043–0.7 μmol/mL for 24 h, and cellular supernatants collected. Human EMMPRIN and MIF levels were measured in the supernatant using the DuoSet® ELISA Development System (Cat. DY972, DY289, R&D Systems, USA). Human IL-1β and IL-8 levels were analyzed in the same supernatants by using the BD OptEIA™ human ELISA Set II (Cat. 557953, 555244, BD Bioseciences, USA). All the assays were performed according to the manufacturers' instructions. Absorbance was measured at 450 nm with a SpectraMax M5 microplate spectrophotometer and the cytokine quantities were calculated through the use of standard curves for each recombinant cytokine.

Assessment of Acute and Sub-acute Pulmonary Responses to III-V Materials in the Murine Lung

Eight-week-old male C57BL/6 mice were purchased from Charles River Laboratories (Hollister, CA, USA). The animal experiments followed standard procedures for animal housing (filter-topped cages; room temperature at 23 ± 2 °C; 60% relative humidity; 12 h light, 12 h dark cycle) and hygiene status (autoclaved food and acidified water). Each group included 6 animals. Animal exposure was carried out by an oropharyngeal aspiration method developed at NIOSH. Briefly, all the particles and ion solutions were freshly suspended in PBS to keep the particle and ionic concentrations at 0.014 mmol/kg. Positive control ZnO NPs were used at 0.014 mmol/kg and MUS (Min-U-Sil) at 0.083 mg/kg (Table 3). Under ketamine/xylazine (100/10 mg/kg) anesthesia, the mice received oropharyngeal aspiration of a 50 μL volume of each material suspension at the back of the tongue. The same volume of PBS was used as a control. The mice were sacrificed after 40 h and 21 D exposures to assess acute and sub-acute effects, respectively. The BALF was collected by cannulating the trachea and gently lavaging the lung 3 times with 1 mL sterile PBS. BALF cells were cytospun (600 rpm, 5 min) onto microscopic slides and stained with PROTOCOL™ Hema 3™ Fixative and Solutions to perform differential cell counts. A total of 200 cells were counted on the stained slides, in blinded fashion, to assess the differential cell counts, premised on the well-recognized morphological features of macrophages, neutrophils, eosinophil or lymphocytes. The BALF was also used to determine cytokines and proteins using mouse ELISA kits, including for EMMPRIN (Cat. 205575, Abcam, USA), MMP-9, LIX and MIF (Cat. DY16718, DY443 and DY1978, R&D Systems, USA), IL-1β (Cat. 559603, BD Bioseciences, USA), PDGF-AA (Cat. DAA00B, R&D Systems, USA) and TGF-β1 (Cat. G7590, Promega Corporation, Madison, WI, USA). All the ELISA experiments were performed in triplicate, according to the manufacturer's instructions.

Histological Analysis

Lung tissue, harvested at 40 h and 21 D, was fixed in 4% paraformaldehyde and embedded in paraffin. The embedded samples were cut into 4-μm-thick sections and stained with

hematoxylin/eosin to visualize inflammatory infiltrates or Masson's trichrome stain to visualize collagen deposition in the lung, respectively.

Sircol Assay for Total Collagen Quantification

The right lobes of lungs collected after 21 D were homogenized for 3 minutes in PBS at 50 mg tissue per ml, using a tissue homogenizer (Fisher Scientific, USA). 100 μL of each sample was transferred into low protein-binding microtubes, followed by adding 400 μL acetic acid (0.5 M) and pepsin (0.1 mg/mL in 0.5 M acetic acid) for overnight incubation at 4 °C. Cellular debris was pelleted by 10 min centrifugation at 3500rpm. 30 μL supernatant from each sample was analyzed for total protein content, using the Quick Start™ Bradford Protein Assay (BIO-RAD, USA) according to the manufacturer's instructions. The remaining 470 μL supernatant was used for collagen extraction by the Sircol™ Soluble Collagen Assay kit (Biocolor Ltd., Carrickfergus, UK) according to the manufacturer's instructions. Similar prepared collagen standards (0–50 μg) were run in parallel. After collecting the collagen pellets and adding alkali reagent, absorbance was read at 555 nm in a plate reader (SpectraMax M5 microplate, Molecular Devices Corp., Sunnyvale, CA). Data were normalized by total protein content and expressed as μg of soluble collagen per mg of lung protein.

ICP-OES Analysis to Determine III-V Content in the Murine Lung

ICP-OES analysis was used to detect the presence of III-V elements in the mice lung at 40 h and 21 D exposure. The intact lungs were collected and homogenized for 3 minutes in 1.5 mL PBS with a tissue homogenizer (Fisher Scientific, USA). The total protein content in each sample was determined by the Quick Start™ Bradford Protein Assay. All the homogenates were transferred to Teflon containers and digested with concentrated HNO_3 and hydrogen peroxide at 80 °C for 6 h, followed by liquid evaporation at 95 °C. The dried samples were diluted with 2% (v/v) nitric acid for 3 h to extract the analytes. These extracts were transferred to 15 mL ICP-OES tubes and additional HNO_3 was added to reach a final volume of 8 mL. A calibration curve was established using standard As, Ga and In solutions (Elements Inc., 100 mg/L in 2% HNO_3). Each sample and standard was analyzed in triplicate in the presence of 2% (v/v) nitric acid. The final element content was expressed as μmol of III-Vs/μg of protein.

Statistical Analysis

All the experiments were done in triplicate with results expressed as mean ± standard deviation (SD). Statistical significance was evaluated using two-tailed heteroscedastic Student's t-tests according to the TTEST function in Microsoft Excel. Statistically significant results were considered as $p<0.05$.

Supplementary Material

Refer to Web version on PubMed Central for supplementary material.

Acknowledgments

This work was primarily supported by the US Public Health Service Grant, R01 ES016746, and also leveraged the Characterization Core of the UC-CEIN, funded by the National Science Foundation (Cooperative agreement Number DBI-1266377). Funding and materials were provided by Semiconductor Research Corporation (SRC) Engineering Research Center for Environmentally Benign Semiconductor Manufacturing (task ID 425.050). Any opinions, findings, conclusions or recommendations expressed herein are those of the author(s).

REFERENCES AND NOTES

1. Fan GY, Wang CY, Fang JY. Solution-based Synthesis of III-V Quantum Dots and Their Applications in Gas Sensing and Bio-imaging. Nano Today. 2014; 9:69–84.
2. Tomioka K, Ikejiri K, Tanaka T, Motohisa J, Hara S, Hiruma K, Fukui T. Selective-area Growth of III-V Nanowires and Their Applications. J. Mater. Res. 2011; 26:2127–2141.
3. Speed D, Westerhoff P, Sierra-Alvarez R, Draper R, Pantano P, Aravamudhan S, Chen KL, Hristovski K, Herckes P, Bi X, et al. Physical, Chemical, and *in vitro* Toxicological Characterization of Nanoparticles in Chemical Mechanical Planarization Suspensions Used in the Semiconductor Industry: towards Environmental Health and Safety Assessments. Environ. Sci.: Nano. 2015; 2:227–244.
4. Flaherty NL, Chandrasekaran A, Pena MdPS, Roth GA, Brenner SA, Begley TJ, Melendez JA. Comparative Analysis of Redox and Inflammatory Properties of Pristine Nanomaterials and Commonly Used Semiconductor Manufacturing Nano-Abrasives. Toxicol. Lett. 2015; 239:205–215. [PubMed: 26444223]
5. Chen HW, Chen WY, Chang CN, Chuang YH, Lin YH. Identifying Airborne Metal Particles Sources Near an Optoelectronic and Semiconductor Industrial Park. Atmos. Res. 2016; 174–175:97–105.
6. Darnton A, Miller BG, MacCalman L, Galea KS, Wilkinson S, Cherrie JW, Shafrir A, McElvenny D, Osman J. An Updated Investigation of Cancer Incidence and Mortality at a Scottish Semiconductor Manufacturing Facility with Case-control and Case-Only Studies of Selected Cancers. Occup. Environ. Med. 2012; 69:767–769. [PubMed: 22718705]
7. Brenner SA, Neu-Baker NM, Eastlake AC, Beaucham CC, Geraci CL. NIOSH Field Studies Team Assessment: Worker Exposure to Aerosolized Metal Oxide Nanoparticles in a Semiconductor Fabrication Facility. J. Occup. Environ. Hyg. 2016; 13:871–880. [PubMed: 27171535]
8. Takahashi M, Nishihira J, Shimpo M, Mizue Y, Ueno S, Mano H, Kobayashi E, Ikeda U, Shimada K. Macrophage Migration Inhibitory Factor as a Redox-Sensitive Cytokine in Cardiac Myocytes. Cardiovasc. Res. 2001; 52:438–445. [PubMed: 11738060]
9. Ozaki K, Haseman JK, Hailey JR, Maronpot RR, Nyska A. Association of Adrenal Pheochromocytoma and Lung Pathology in Inhalation Studies with Particulate Compounds in the Male F344 Rat - The National Toxicology Program Experience. Toxicol. Pathol. 2002; 30:263–270. [PubMed: 11950170]
10. Aizawa Y, Takata T, Karube H, Nakamura K, Kotani M. Effects of GaAs and Ga_2O_3 on Magnetometric Behavior of Iron-Oxide Particles in Rabbit Lungs. Appl. Organomet. Chem. 1994; 8:207–213.
11. Tanaka A, Hirata M, Omura M, Zhao M, Makita Y, Yamazaki K, Inoue N, Gotoh K. Comparative Study of the Toxic Effects of Gallium Arsenide, Indium Arsenide and Arsenic Trioxide Following Intratracheal Instillations to the Lung of Syrian Golden Hamsters. Fukuoka Acta Medica. 2000; 91:21–33.
12. Tanaka A, Hisanaga A, Hirata M, Omura M, Makita Y, Inoue N, Ishinishi N. Chronic Toxicity of Indium Arsenide and Indium Phosphide to the Lungs of Hamsters. Fukuoka Acta Medica. 1996; 87:108–115.
13. Jiang W, Lin S, Chang CH, Ji Z, Sun B, Wang X, Li R, Pon N, Xia T, Nel AE. Implications of the Differential Toxicological Effects of III-V Ionic and Particulate Materials for Hazard Assessment of Semiconductor Slurries. Acs Nano. 2015; 9:12011–12025. [PubMed: 26549624]

14. NTP Toxicology and Carcinogenesis Studies of Gallium Arsenide (CAS No. 1303-00-0) in F344/N Rats and B6C3F1 Mice (Inhalation Studies). Natl. Toxicol. Program Tech. Rep. Ser. 2000; 492:1–306. [PubMed: 12563348]
15. Caffrey-Nolan RE, McCoy KL. Direct Exposure to Gallium Arsenide Upregulates Costimulatory Activity of Murine Macrophages. Toxicol. Appl. Pharmacol. 1998; 151:330–339. [PubMed: 9707509]
16. Sikorski EE, Burns LA, Stern ML, Luster MI, Munson AE. Splenic Cell Targets in Gallium Arsenide-Induced Suppression of the Primary Antibody-Response. Toxicol. Appl. Pharmacol. 1991; 110:129–142. [PubMed: 1871769]
17. Webb DR, Wilson SE, Carter DE. Comparative Pulmonary Toxicity of Gallium-Arsenide, Gallium(III) Oxide, or Arsenic(III) Oxide Intratracheally Instilled into Rats. Toxicol. Appl. Pharmacol. 1986; 82:405–416. [PubMed: 3952726]
18. Webb DR, Sipes IG, Carter DE. *In vitro* Solubility and *in vivo* Toxicity of Gallium Arsenide. Toxicol. Appl. Pharmacol. 1984; 76:96–104. [PubMed: 6484996]
19. Webb DR, Wilson SE, Carter DE. Pulmonary Clearance and Toxicity of Respirable Gallium-Arsenide Particulates Intratracheally Instilled into Rats. Am. Ind. Hyg. Assoc. J. 1987; 48:660–667. [PubMed: 3618480]
20. Yamazaki K, Tanaka A, Hirata M, Omura M, Makita Y, Inoue N, Sugio K, Sugimachi K. Long Term Pulmonary Toxicity of Indium Arsenide and Indium Phosphide Instilled Intratracheally in Hamsters. J. Occup. Health. 2000; 42:169–178.
21. Blazka ME, Tepper JS, Dixon D, Winsett DW, O'Connor RW, Luster MI. Pulmonary Response of Fischer 344 Rats to Acute Nose-Only Inhalation of Indium Trichloride. Environ. Res. 1994; 67:68–83. [PubMed: 7925195]
22. Blazka ME, Dixon D, Haskins E, Rosenthal GJ. Pulmonary Toxicity to Intratracheally Administered Indium Trichloride in Fischer-344 Rats. Fundam. Appl. Toxicol. 1994; 22:231–239. [PubMed: 8005375]
23. Luo JCJ, Hsu KH, Hsieh LL, Wong CJ, Chang MJW. Lung Function and General Illness Symptoms in a Semiconductor Manufacturing Facility. J. Occup. Environ. Med. 1998; 40:895–900. [PubMed: 9800175]
24. Luo JCJ, Hsieh LL, Chang MJW, Hsu KH. Decreased White Blood Cell Counts in Semiconductor Manufacturing Workers in Taiwan. Occup. Environ. Med. 2002; 59:44–48. [PubMed: 11836468]
25. McElvenny DM, Darnton AJ, Hodgson JT, Clarke SD, Elliott RC, Osman J. Investigation of Cancer Incidence and Mortality at a Scottish Semiconductor Manufacturing Facility. Occup. Med. 2003; 53:419–430.
26. Darnton A, Wilkinson S, Miller B, MacCalman L, Galea K, Shafrir A, Cherrie J, McElvenny D, Osman J. A Further Study of Cancer among the Current and Former Employees of National Semiconductor (UK) Ltd. Greenock. Sudbury, Suffolk (UK): Health and Safety Executive and Institute of Occupational Medicine. 2010:135.
27. Wang X, Ji Z, Chang CH, Zhang H, Wang M, Liao YP, Lin S, Meng H, Li R, Sun B, et al. Use of Coated Silver Nanoparticles to Understand the Relationship of Particle Dissolution and Bioavailability to Cell and Lung Toxicological Potential. Small. 2014; 10:385–398. [PubMed: 24039004]
28. Zhang H, Ji Z, Xia T, Meng H, Low-Kam C, Liu R, Pokhrel S, Lin S, Wang X, Liao YP, et al. Use of Metal Oxide Nanoparticle Band Gap To Develop a Predictive Paradigm for Oxidative Stress and Acute Pulmonary Inflammation. Acs Nano. 2012; 6:4349–4368. [PubMed: 22502734]
29. Flora SJ, Bhatt K, Dwivedi N, Pachauri V, Kushwah PK. Co-administration of Meso 2,3-dimercaptosuccinic Acid Monoesters Reduces Arsenic Concentration and Oxidative Stress in Gallium Arsenide Exposed Rats. Clin. Exp. Pharmacol. Physiol. 2011; 38:423–429. [PubMed: 21501211]
30. Xia T, Kovochich M, Liong M, Maedler L, Gilbert B, Shi H, Yeh JI, Zink JI, Nel AE. Comparison of the Mechanism of Toxicity of Zinc Oxide and Cerium Oxide Nanoparticles Based on Dissolution and Oxidative Stress Properties. Acs Nano. 2008; 2:2121–2134. [PubMed: 19206459]
31. Hahn JN, Kaushik DK, Yong VW. The Role of EMMPRIN in T Cell Biology and Immunological Diseases. J. Leukocyte Biol. 2015; 98:33–48. [PubMed: 25977287]

32. Sauler M, Bucala R, Lee PJ. Role of Macrophage Migration Inhibitory Factor in Age-Related Lung Disease. Am. J. Physiol.: Lung Cell. Mol. Physiol. 2015; 309:L1–L10. [PubMed: 25957294]
33. Cobalt in Hard Metals and Cobalt Sulfate, Gallium Arsenide, Indium Phosphide and Vanadium Pentoxide. IARC Monogr. Eval. Carcinog. Risks Hum. 2006; 86:1–294. [PubMed: 16906675]
34. Sheehy JW, Jones JH. Assessment of Arsenic Exposures and Controls in Gallium Arsenide Production. Am. Ind. Hyg. Assoc. J. 1993; 54:61–69. [PubMed: 8452098]
35. Sienel W, Polzer B, Elshawi K, Lindner M, Morresi-Hauf A, Vay C, Eder F, Passlick B, Klein CA. Cellular Localization of EMMPRIN Predicts Prognosis of Patients with Operable Lung Adenocarcinoma Independent from MMP-2 and MMP-9. Mod. Pathol. 2008; 21:1130–1138. [PubMed: 18567995]
36. Herold S, Mayer K, Lohmeyer J. Acute Lung Injury: How Macrophages Orchestrate Resolution of Inflammation and Tissue Repair. Front Immunol. 2011; 2:82. [PubMed: 22566871]
37. Kim JH, Suk MH, Yoon DW, Lee SH, Hur GY, Jung KH, Jeong HC, Lee SY, Suh IB, Shin C, et al. Inhibition of Matrix Metalloproteinase-9 Prevents Neutrophilic Inflammation in Ventilator-Induced Lung Injury. Am. J. Physiol.: Lung Cell. Mol. Physiol. 2006; 291:L580–587. [PubMed: 16698855]
38. Geiser M. Update on Macrophage Clearance of Inhaled Micro- and Nanoparticles. J. Aerosol Med. Pulm. Drug Delivery. 2010; 23:207–217.
39. Doshi N, Mitragotri S. Macrophages Recognize Size and Shape of Their Targets. Plos One. 2010; 5:e10051. [PubMed: 20386614]
40. Hirota K, Terada H. Endocytosis of Particle Formulations by Macrophages and Its Application to Clinical Treatment. Mol. Regul. Endocytosis. 2012:413–428.
41. Li R, Ji Z, Chang CH, Dunphy DR, Cai X, Meng H, Zhang H, Sun B, Wang X, Dong J, et al. Surface Interactions with Compartmentalized Cellular Phosphates Explain Rare Earth Oxide Nanoparticle Hazard and Provide Opportunities for Safer Design. Acs Nano. 2014; 8:1771–1783. [PubMed: 24417322]
42. Wang X, Duch MC, Mansukhani N, Ji Z, Liao YP, Wang M, Zhang H, Sun B, Chang CH, Li R, et al. Use of a Pro-Fibrogenic Mechanism-Based Predictive Toxicological Approach for Tiered Testing and Decision Analysis of Carbonaceous Nanomaterials. Acs Nano. 2015; 9:3032–3043. [PubMed: 25646681]
43. Wang X, Xia T, Duch MC, Ji ZX, Zhang HY, Li RB, Sun BB, Lin SJ, Meng H, Liao YP, et al. Pluronic F108 Coating Decreases the Lung Fibrosis Potential of Multiwall Carbon Nanotubes by Reducing Lysosomal Injury. Nano Lett. 2012; 12:3050–3061. [PubMed: 22546002]
44. Nel AE. Implementation of Alternative Test Strategies for the Safety Assessment of Engineered Nanomaterials. J. Intern. Med. 2013; 274:561–577. [PubMed: 23879741]
45. Kim JY, Kim WJ, Kim H, Suk K, Lee WH. The Stimulation of CD147 Induces MMP-9 Expression through ERK and NF-kappaB in Macrophages: Implication for Atherosclerosis. Immune network. 2009; 9:90–97. [PubMed: 20107538]
46. Veillat V, Lavoie CH, Metz CN, Roger T, Labelle Y, Akoum A. Involvement of nuclear factor-kappaB in macrophage migration inhibitory factor gene transcription up-regulation induced by interleukin- 1 beta in ectopic endometrial cells. Fertil Steril. 2009; 91:2148–2156. [PubMed: 18710704]
47. Meng, XG., Wang, W. Speciation of Arsenic by Disposable Cartridges; Book of Posters of the Third International Conference on Arsenic Exposure and He and Health Effects Society of Environmental Geochemistry and Health Denver Colorado; 1998.
48. Barchowsky A, Dudek EJ, Treadwell MD, Wetterharn KE. Arsenic induces oxidant stress and NF-kappa B activation in cultured aortic endothelial cells. Free Radical Biol. Med. 1996; 21:783–790. [PubMed: 8902524]
49. Eblin KE. Arsenical-induced Reactive Oxygen Species Lead to Altered Cellular Signaling and Phenotypic Alterations in Human Bladder Cells. 2008 ProQuest.
50. Fry RC, Navasumrit P, Valiathan C, Svensson JP, Hogan BJ, Luo M, Bhattacharya S, Kandjanapa K, Soontararuks S, Nookabkaew S, et al. Activation of inflammation/NF-kappa B signaling in infants born to arsenic-exposed mothers. PLoS Genet. 2007; 3:2180–2189.

51. Yurchenko V, Constant S, Eisenmesser E, Bukrinsky M. Cyclophilin-CD147 Interactions: a New Target for Anti-inflammatory Therapeutics. Clin. Exp. Immunol. 2010; 160:305–317. [PubMed: 20345978]
52. Foda HD, Rollo EE, Drews M, Conner C, Appelt K, Shalinsky DR, Zucker S. Ventilator-Induced Lung Injury Upregulates and Activates Gelatinases and EMMPRIN - Attenuation by the Synthetic Matrix Metalloproteinase Inhibitor, Prinomastat (AG3340). Am. J. Respir. Cell Mol. Biol. 2001; 25:717–724. [PubMed: 11726397]
53. Guillot S, Delaval P, Brinchault G, Caulet-Maugendre S, Depince A, Lena H, Delatour B, Lagente V, Martin-Chouly C. Increased Extracellular Matrix Metalloproteinase Inducer (EMMPRIN) Expression in Pulmonary Fibrosis. Exp. Lung Res. 2006; 32:81–97. [PubMed: 16754474]
54. Zernecke A, Bernhagen J, Weber C. Macrophage Migration Inhibitory Factor in Cardiovascular Disease. Circulation. 2008; 117:1594–1602. [PubMed: 18362243]
55. Pardo A, Selman M. Matrix Metalloproteases in Aberrant Fibrotic Tissue Remodeling. Proc. Am. Thorac. Soc. 2006; 3:383–388. [PubMed: 16738205]
56. Tanino Y, Makita H, Miyamoto K, Betsuyaku T, Ohtsuka Y, Nishihira J, Nishimura M. Role of Macrophage Migration Inhibitory Factor in Bleomycin-Induced Lung Injury and Fibrosis in Mice. Am. J. Physiol.: Lung Cell. Mol. Physiol. 2002; 283:L156–L162. [PubMed: 12060572]
57. Takahashi K, Koga K, Linge HM, Zhang YZ, Lin XC, Metz CN, Al-Abed Y, Ojamaa K, Miller EJ. Macrophage CD74 Contributes to MIF-induced Pulmonary Inflammation. Respir. Res. 2009; 10:33. [PubMed: 19413900]
58. Gao L, Flores C, Fan-Ma S, Miller EJ, Moitra J, Moreno L, Wadgaonkar R, Simon B, Brower R, Sevransky J, et al. Macrophage Migration Inhibitory Factor in Acute Lung Injury: Expression, Biomarker, and Associations. Transl. Res. 2007; 150:18–29. [PubMed: 17585860]
59. Onodera S, Kaneda K, Mizue Y, Koyama Y, Fujinaga M, Nishihira J. Macrophage Migration Inhibitory Factor Up-regulates Expression of Matrix Metalloproteinases in Synovial Fibroblasts of Rheumatoid Arthritis. J. Biol. Chem. 2000; 275:444–450. [PubMed: 10617637]
60. Yu X, Lin SG, Huang XR, Bacher M, Leng L, Bucala R, Lan HY. Macrophage Migration Inhibitory Factor Induces MMP-9 Expression in Macrophages *via* the MEK-ERK MAP Kinase Pathway. J. Interferon Cytokine Res. 2007; 27:103–109. [PubMed: 17316137]
61. Kong YZ, Yu X, Tang JJ, Ouyang X, Huang XR, Fingerle-Rowson G, Bacher M, Scher LA, Bucala R, Lan HY. Macrophage Migration Inhibitory Factor Induces MMP-9 Expression: Implications for Destabilization of Human Atherosclerotic Plaques. Atherosclerosis. 2005; 178:207–215. [PubMed: 15585220]
62. Davey A, McAuley DF, O'Kane CM. Matrix Metalloproteinases in Acute Lung Injury: Mediators of Injury and Drivers of Repair. Eur. Respir. J. 2011; 38:959–970. [PubMed: 21565917]
63. Atkinson JJ, Senior RM. Matrix Metalloproteinase-9 in Lung Remodeling. Am. J. Respir. Cell Mol. Biol. 2003; 28:12–24. [PubMed: 12495928]
64. Albaiceta GM, Gutierrez-Fernandez A, Parra D, Astudillo A, Garcia-Prieto E, Taboada F, Fueyo A. Lack of Matrix Metalloproteinase-9 Worsens Ventilator-induced Lung Injury. Am. J. Physiol.: Lung Cell. Mol. Physiol. 2008; 294:L535–543. [PubMed: 18223162]
65. Hu J, Van den Steen PE, Sang QX, Opdenakker G. Matrix Metalloproteinase Inhibitors as Therapy for Inflammatory and Vascular Diseases. Nat. Rev. Drug Discovery. 2007; 6:480–498. [PubMed: 17541420]
66. Brenner SA, Neu-Baker NM. Occupational Exposure to Nanomaterials: Assessing the Potential for Cutaneous Exposure to Metal Oxide Nanoparticles in a Semiconductor Facility. J. Chem. Health Saf. 2015; 22:10–19.
67. Choi KM, Kim JH, Park JH, Kim KS, Bae GN. Exposure Characteristics of Nanoparticles as Process By-Products for the Semiconductor Manufacturing Industry. J. Occup. Environ. Hyg. 2015; 12:D153–D160. [PubMed: 25751663]
68. Torrance KW, Keenan HE, Hursthouse AS, Stirling D. Measurement of Arsenic and Gallium Content of Gallium Arsenide Semiconductor Waste Streams by ICP-MS. Journal of Environmental Science and Health Part a-Toxic/Hazardous Substances & Environmental Engineering. 2010; 45:471–475.

69. Park D, Yang H, Jeong J, Ha K, Choi S, Kim C, Yoon C, Park D, Paek D. A Comprehensive Review of Arsenic Levels in the Semiconductor Manufacturing Industry. Ann. Occup. Hyg. 2010; 54:869–879. [PubMed: 20724556]

70. Hinderliter PM, Minard KR, Orr G, Chrisler WB, Thrall BD, Pounds JG, Teeguarden JG. ISDD: A Computational Model of Particle Sedimentation, Diffusion and Target Cell Dosimetry for *in vitro* Toxicity Studies. Part. Fibre Toxicol. 2010; 7:36. [PubMed: 21118529]

71. Sun BB, Wang X, Liao YP, Ji ZX, Chang CH, Pokhrel S, Ku J, Liu XS, Wang M, Dunphy DR, et al. Repetitive Dosing of Fumed Silica Leads to Profibrogenic Effects through Unique Structure-Activity Relationships and Biopersistence in the Lung. Acs Nano. 2016; 10:8054–8066. [PubMed: 27483033]

72. Shepard M, Brenner S. Cutaneous Exposure Scenarios for Engineered Nanoparticles Used in Semiconductor Fabrication: a Preliminary Investigation of Workplace Surface Contamination. Int. J. Occup. Environ. Health. 2014; 20:247–257. [PubMed: 25000112]

73. Brenner SA, Neu-Baker NM, Caglayan C, Zurbenko IG. Occupational Exposure to Airborne Nanomaterials: an Assessment of Worker Exposure to Aerosolized Metal Oxide Nanoparticles in Semiconductor Wastewater Treatment. J. Occup. Environ. Hyg. 2015; 12:469–481. [PubMed: 25738602]

74. Marques MRC, Loebenberg R, Almukainzi M. Simulated Biological Fluids with Possible Application in Dissolution Testing. Dissolut Technol. 2011; 18:15–28.

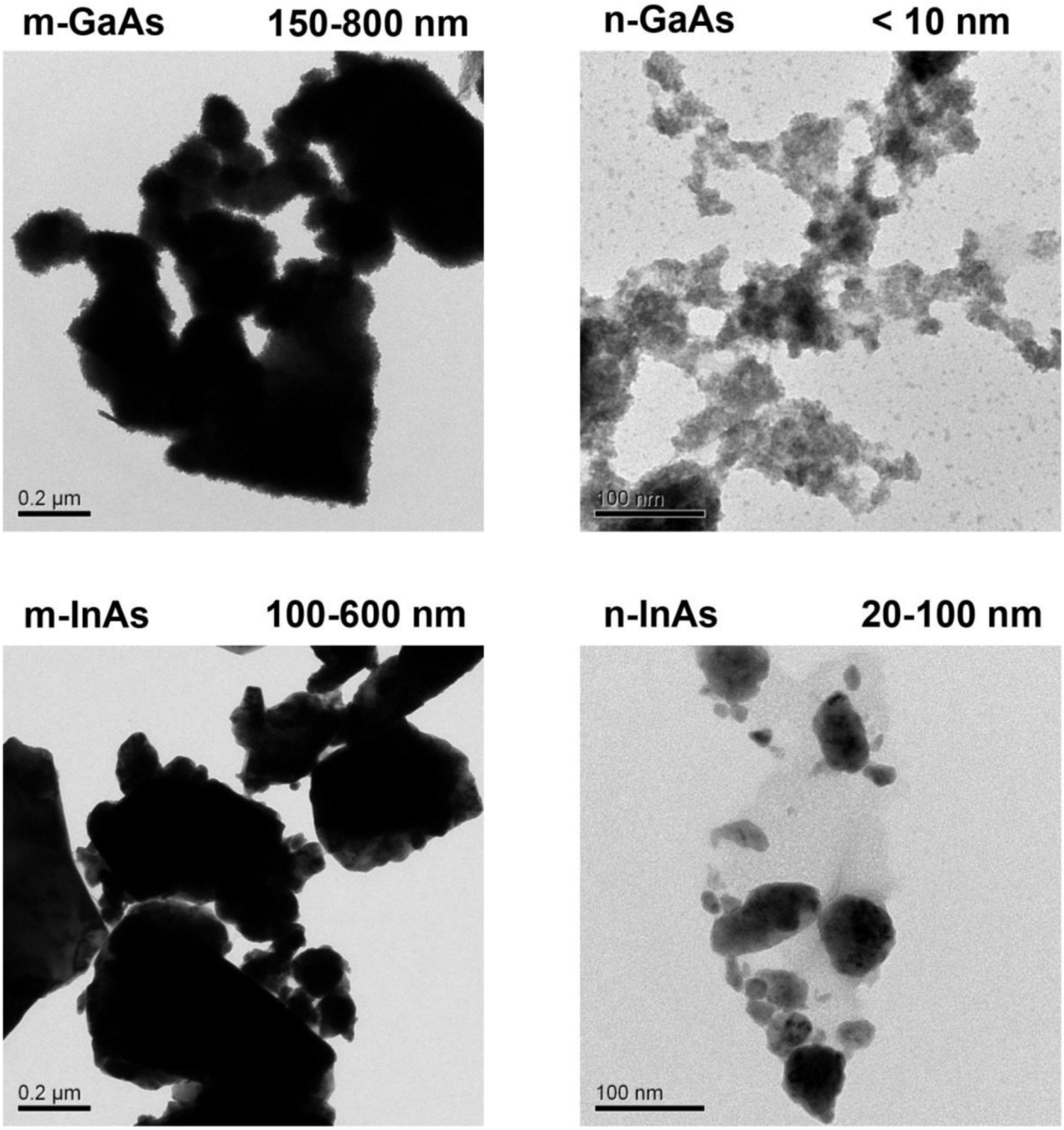

Figure 1.

TEM characterization of micron- and nano-sized GaAs and InAs particles. The particles were suspended at 50 μg/mL and applied to TEM grids. Images were taken using a JEOL 2010 microscope operated at 200 keV. Scale bars represent 0.2 μm for micron-sized particles, and 100 nm for nano-sized particles.

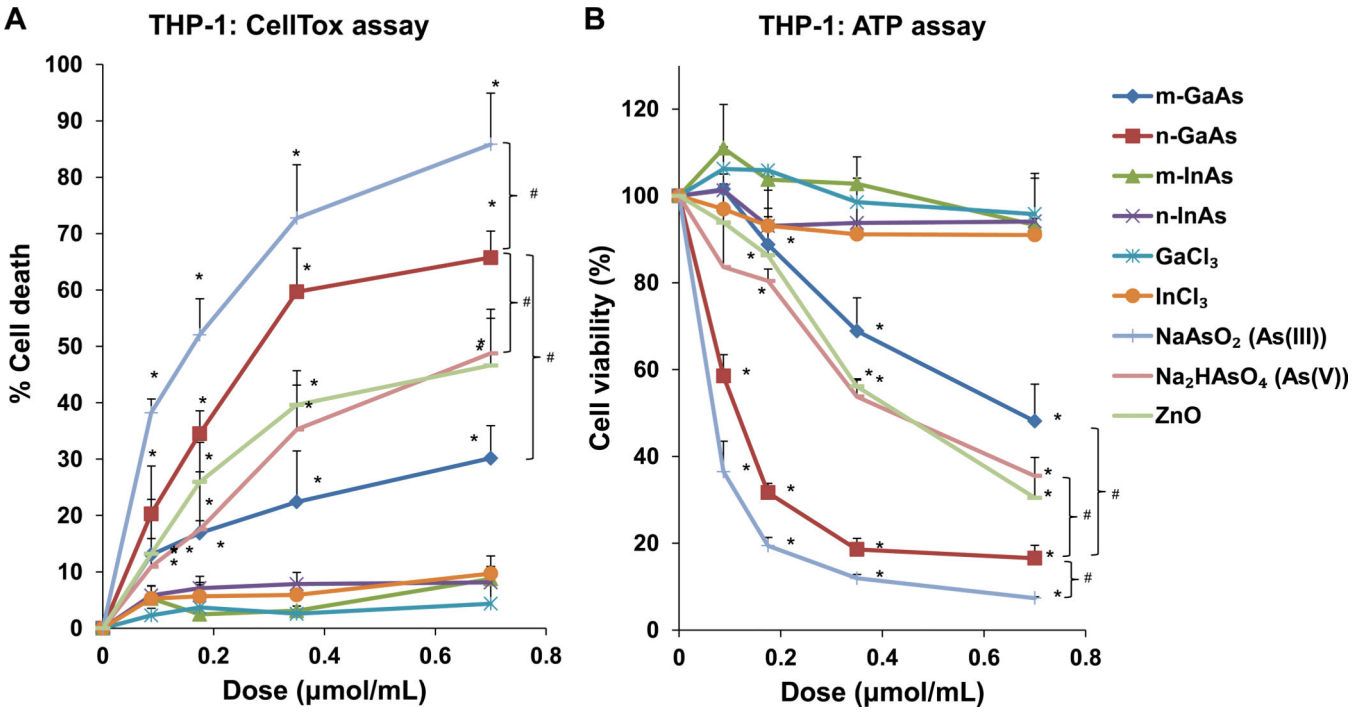

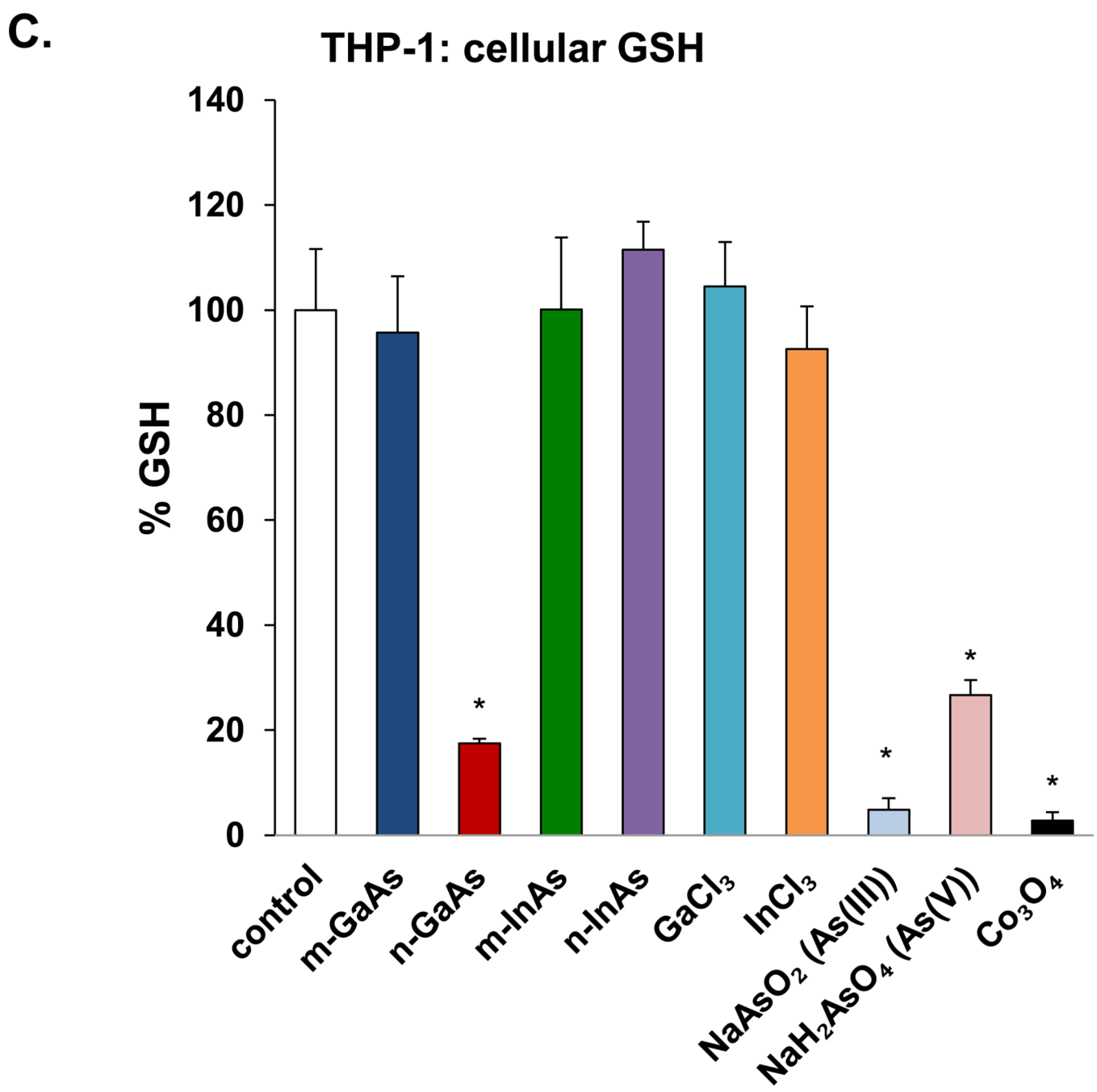

Figure 2.

Cell viability and oxidative stress analysis in THP-1 cells, following treatment with particulate and ionic materials. (A) Assessment of cell death by the CellTox assay. (B) Assessment of THP-1 viability by the ATP assay. The materials were added to the cell culture medium at 0.07–0.7 μmol/mL for 24 h. The corresponding mass doses are listed in Table 3. (*) $p < 0.05$ compared to control; (#) $p < 0.05$ compared to n-GaAs. (C) Intracellular GSH depletion was determined by a luminescence-based GSH-Glo kit. THP-1 cells were exposed to III-V materials at 0.35 μmol/mL (=50 μg/mL GaAs) for 24 h. GSH abundance was calculated as the fractional luminescence intensity of treated *vs.* untreated

cells. The relative GSH abundance in non-treated cells was regarded as 1.0. (*) $p < 0.05$ compared to control.

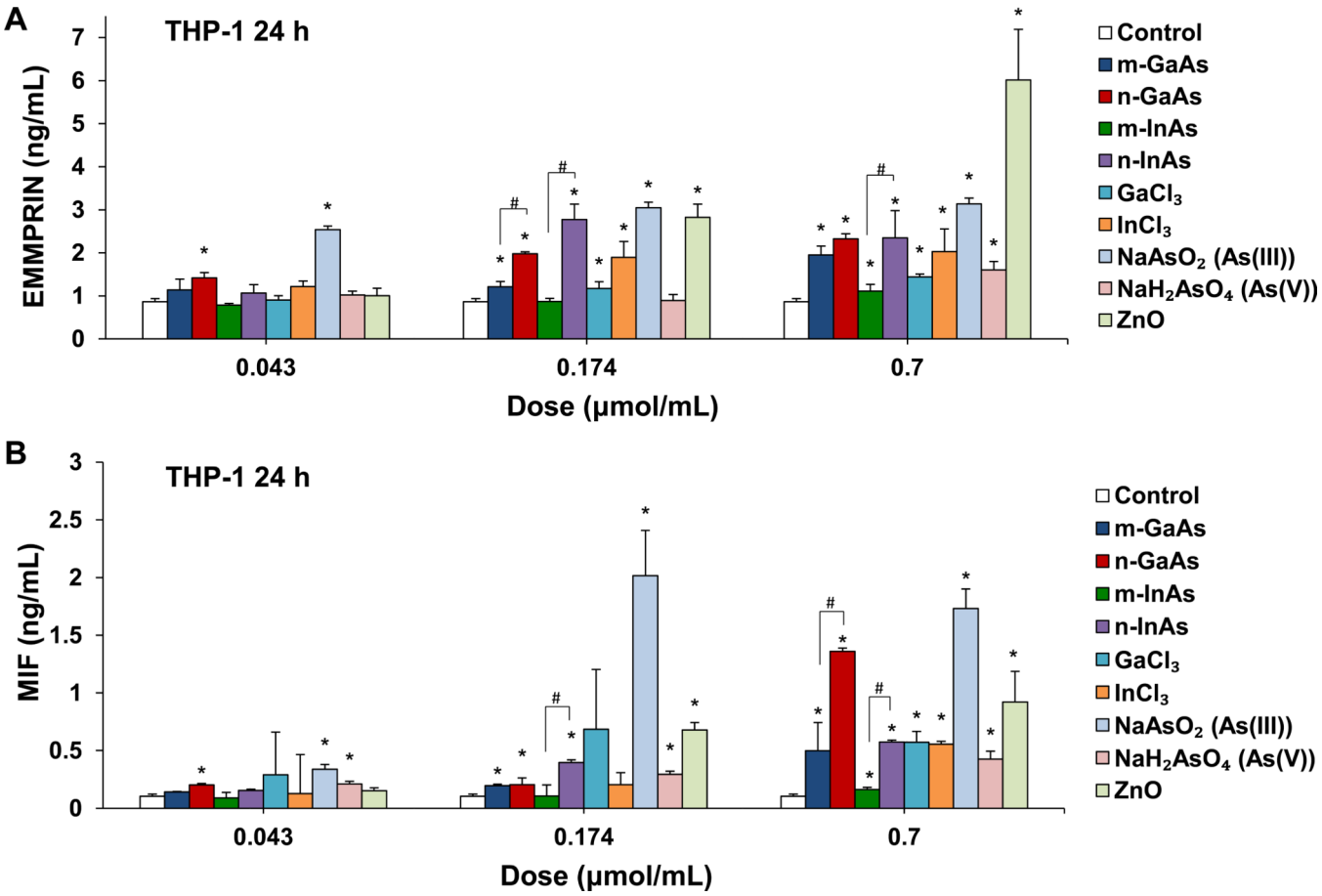

Figure 3.

Comparative effects on EMMPRIN and MIF production in THP-1, following exposure to particulate and ionic III-V materials at 0.043, 0.174 and 0.7 μmol/mL for 24 h. The corresponding mass doses were listed in Table 3. ZnO NPs were used as a positive control. EMMPRIN (A) and MIF (B) levels were assessed in the cell culture supernatant by ELISA. (*) $p < 0.05$ compared to control. (#) $p < 0.05$ compared to nano-sized III-V particles.

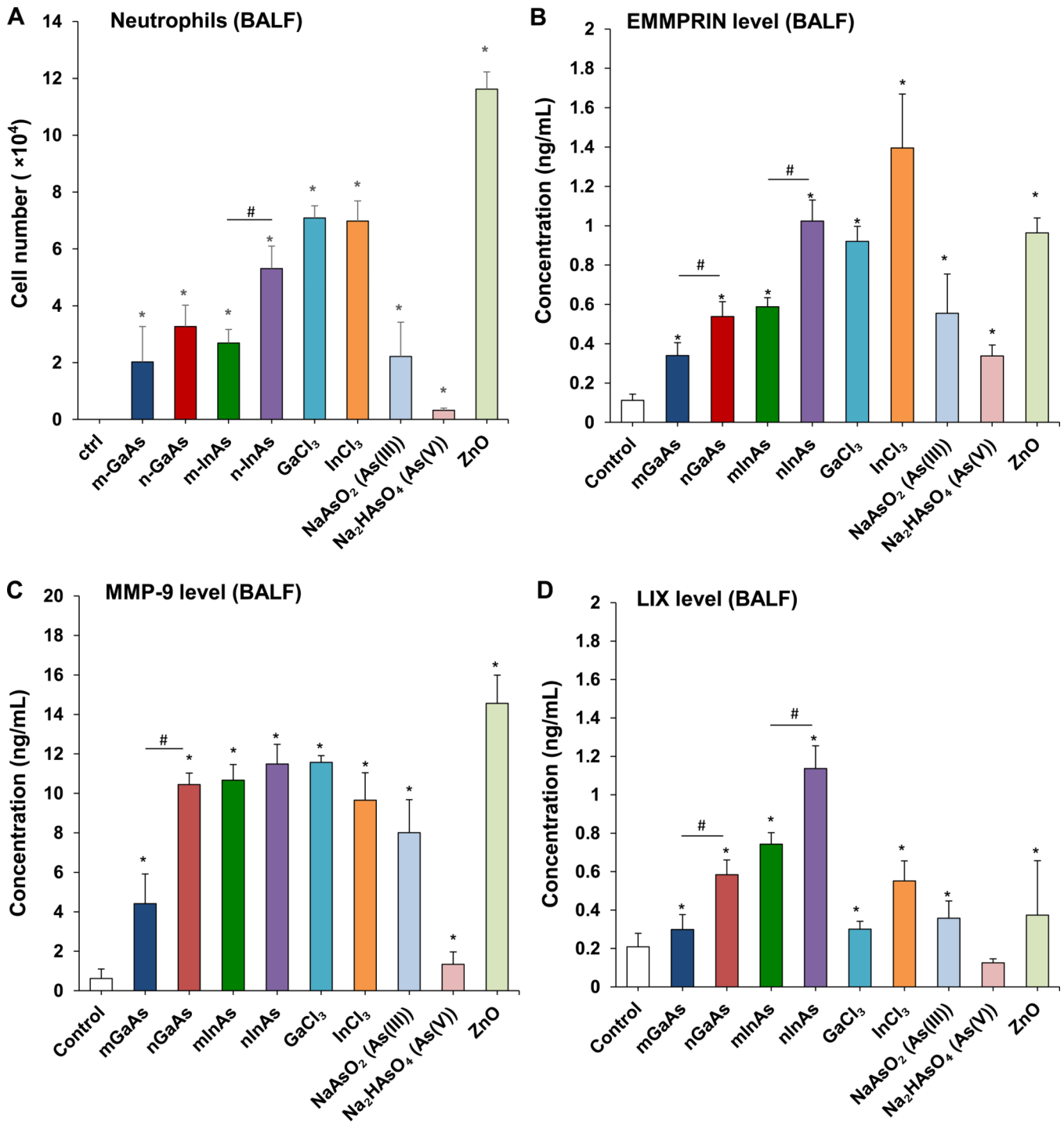

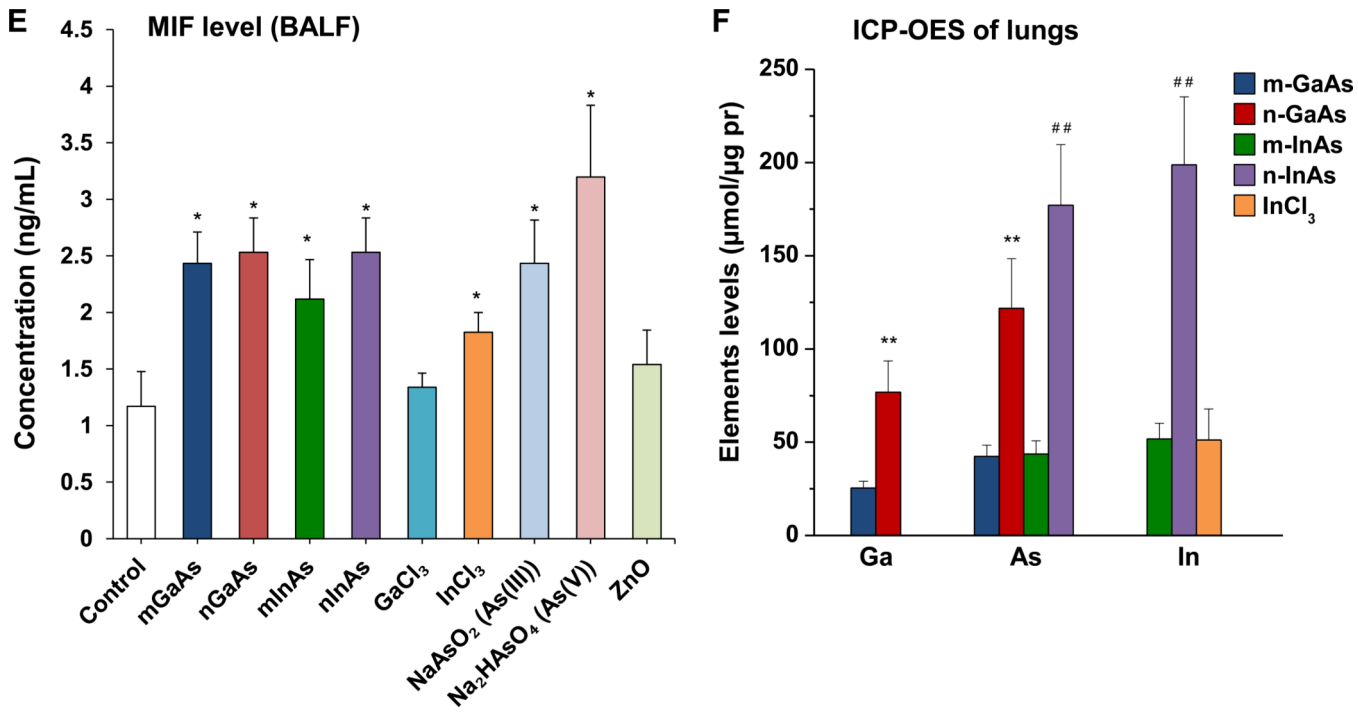

Figure 4.

Acute pulmonary effects of III-V materials in mice after exposure for 40 h. Anesthetized C57BL/6 mice were exposed to III-V particles and ionic forms by a one-time oropharyngeal aspiration of 0.014 mmol/kg (=2 mg/kg GaAs). The corresponding mass doses are listed in Table 3. There were 6 mice per group. Mice were euthanized after 40 h and BALF was collected to determine (A) neutrophil cell counts, (B) EMMPRIN, (C) MMP-9, (D) LIX and (E) MIF levels. (*) $p < 0.05$ compared to control. (#) $p < 0.05$ compared to nano-sized III-V particles. (F) Uptake of III-V materials in the lung tissue was reflected by ICP-OES analysis of Ga, As and In levels, normalized for protein content. The intact lungs were collected and digested by concentrated nitric acid and hydrogen peroxide before determining the elemental content by ICP-OES. No III-V element was detected in the lung tissues of animals exposed to ionic $GaCl_3$, As(III) and As(V). (**) $p < 0.05$ compared to m-GaAs. (##) $p < 0.05$ compared to m-InAs.

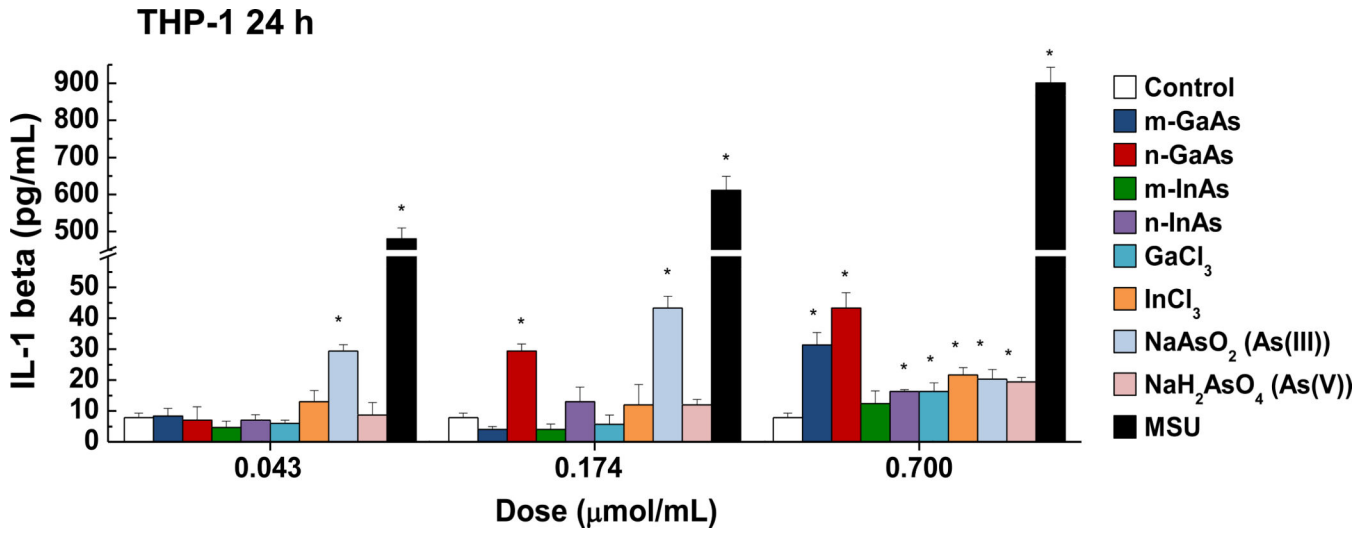

Figure 5.

Assessment of IL-1β production in differentiated THP-1 cells exposed to III-V particles and ionic materials. Three doses (0.043, 0.174 and 0.7 μmol/mL) were tested over 24 h to assess IL-1β release in the cell culture supernatant by ELISA. MSU served as a positive control. (*) $p < 0.05$ compared to control. (#) $p < 0.05$ compared to n-GaAs.

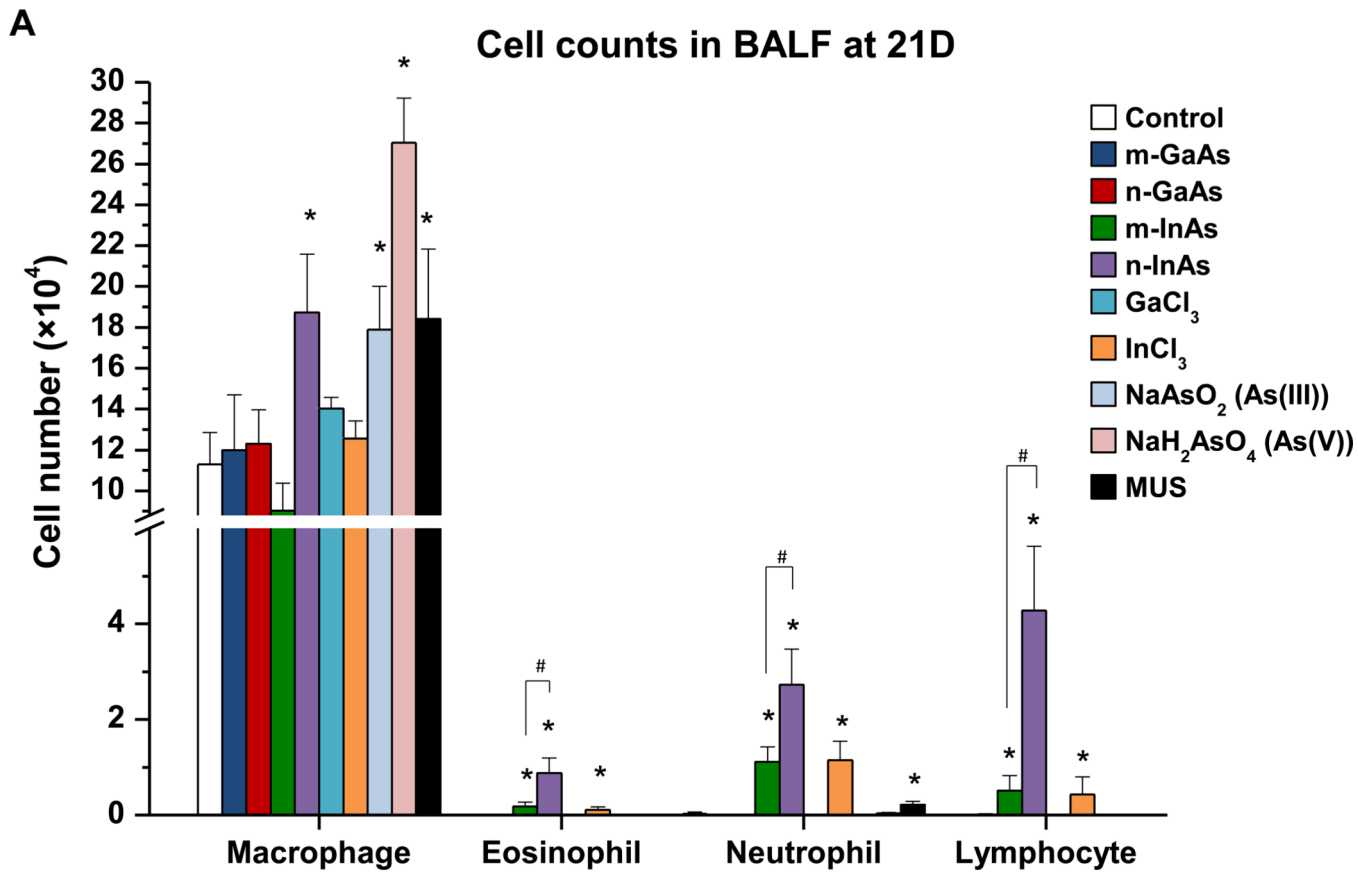

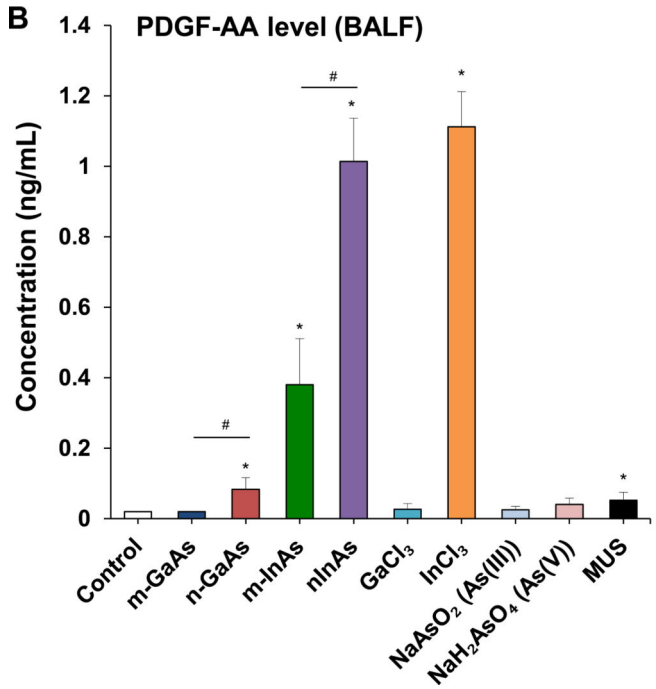

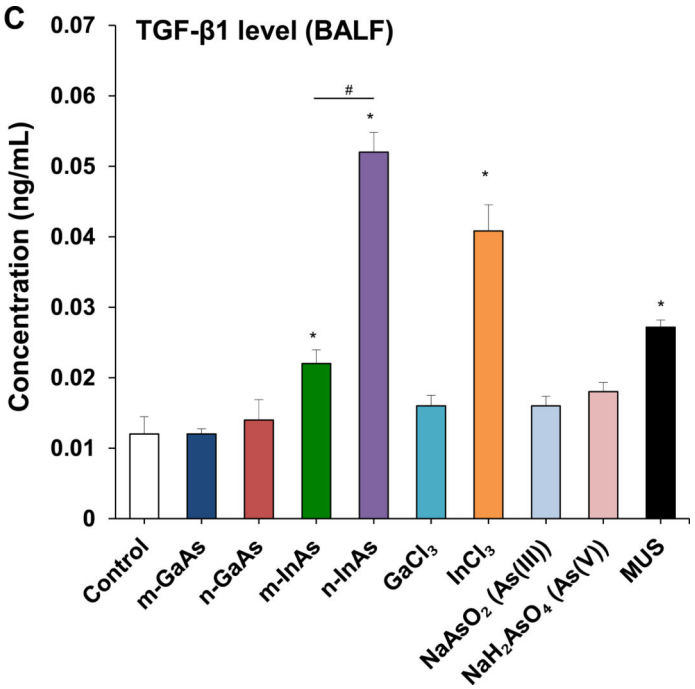

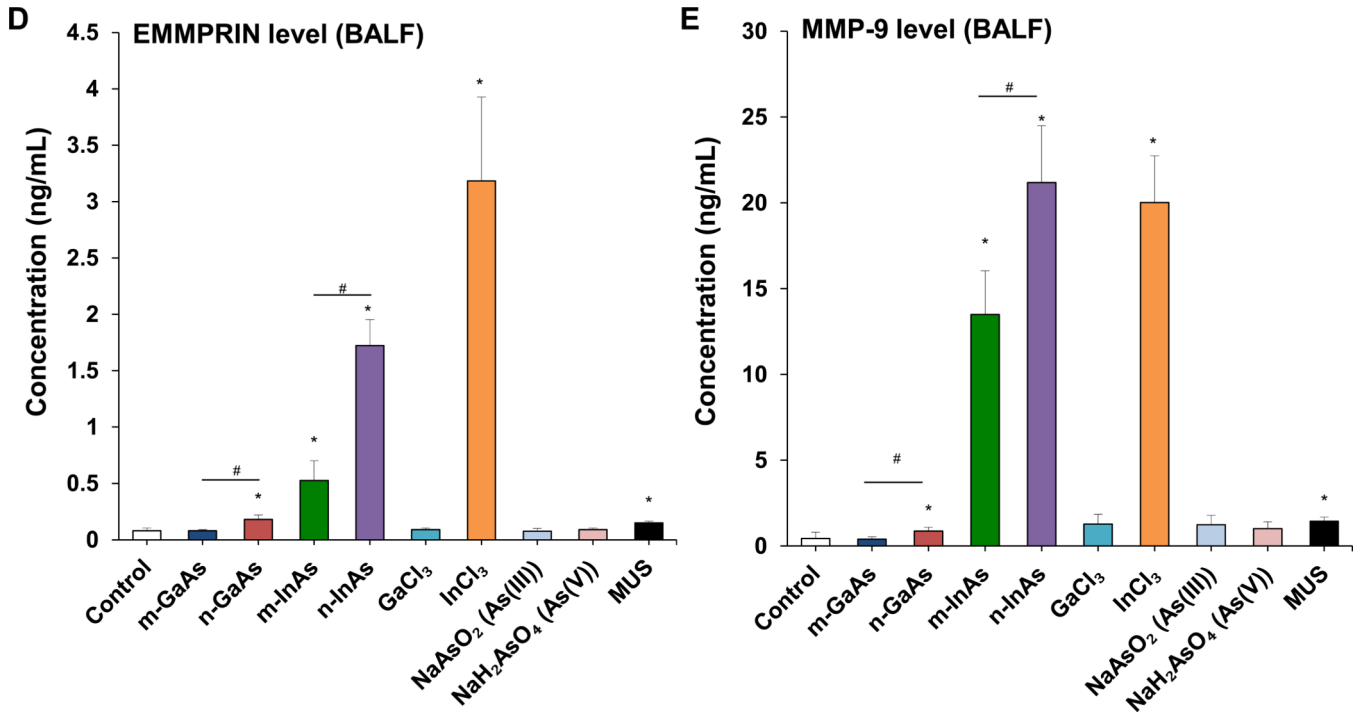

Figure 6.

Assessment of sub-acute lung injury potential of III-V materials in the murine lung, 21 D after initial exposure. The experiment was performed similar to the methods in Figure 4, except that the mice were sacrificed 21 D after the oropharyngeal aspiration of III-V particles and ionic forms at a dose of 0.014 mmol/kg (=2 mg/kg GaAs). The corresponding mass doses are listed in Table 3. The BALF was collected to assess (A) differential cell counts, including macrophages, eosinophils, neutrophils and lymphocytes, (B) pro-fibrogenic PDGF-AA and (C) TGF-β1 levels by ELISA. (D) EMMPRIN and (E) MMP-9 levels were also assessed by ELISA. MUS served as a positive control. (*) $p < 0.05$ compared to control. (#) $p < 0.05$ compared to nano-sized III-V particles.

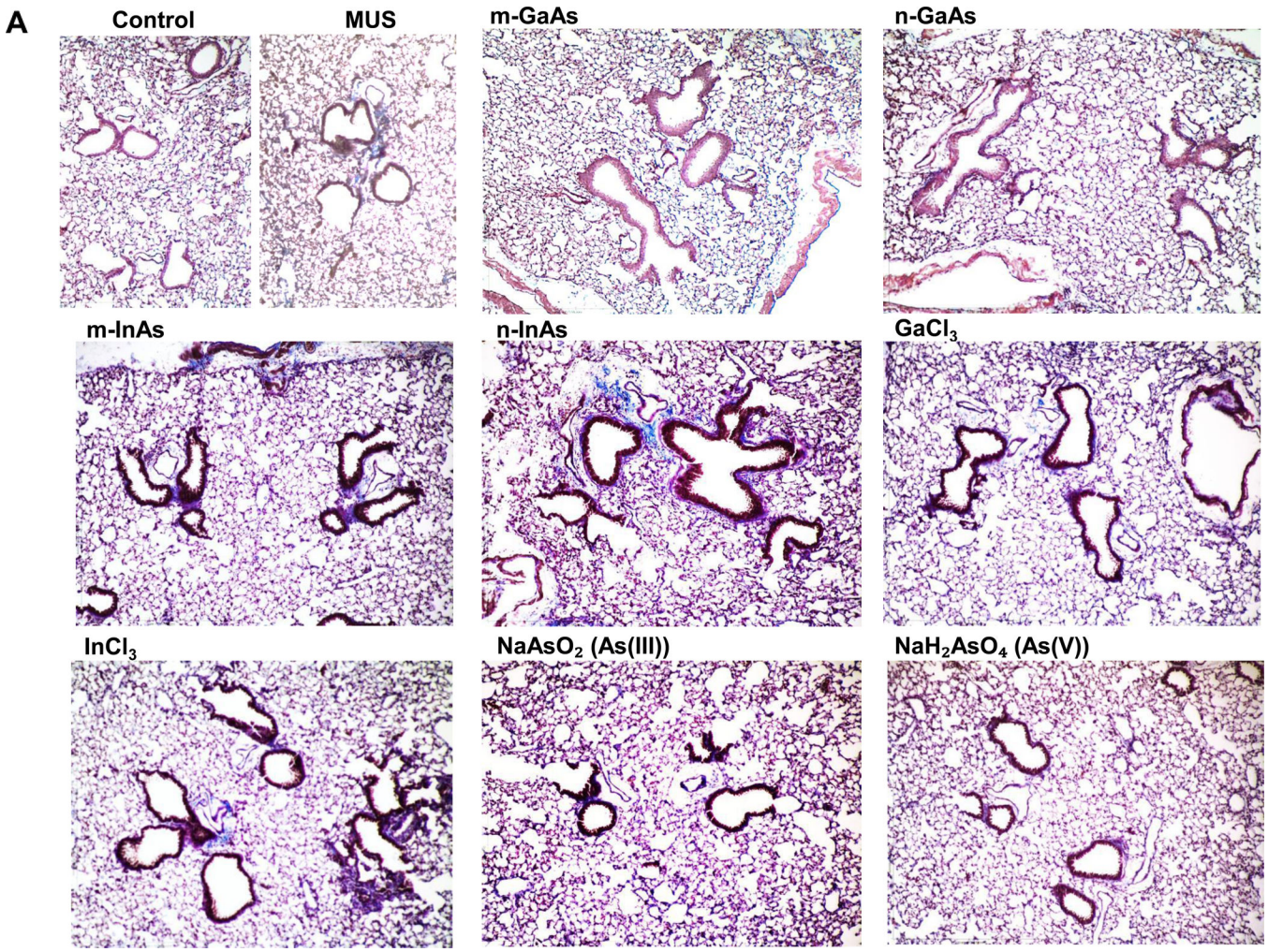

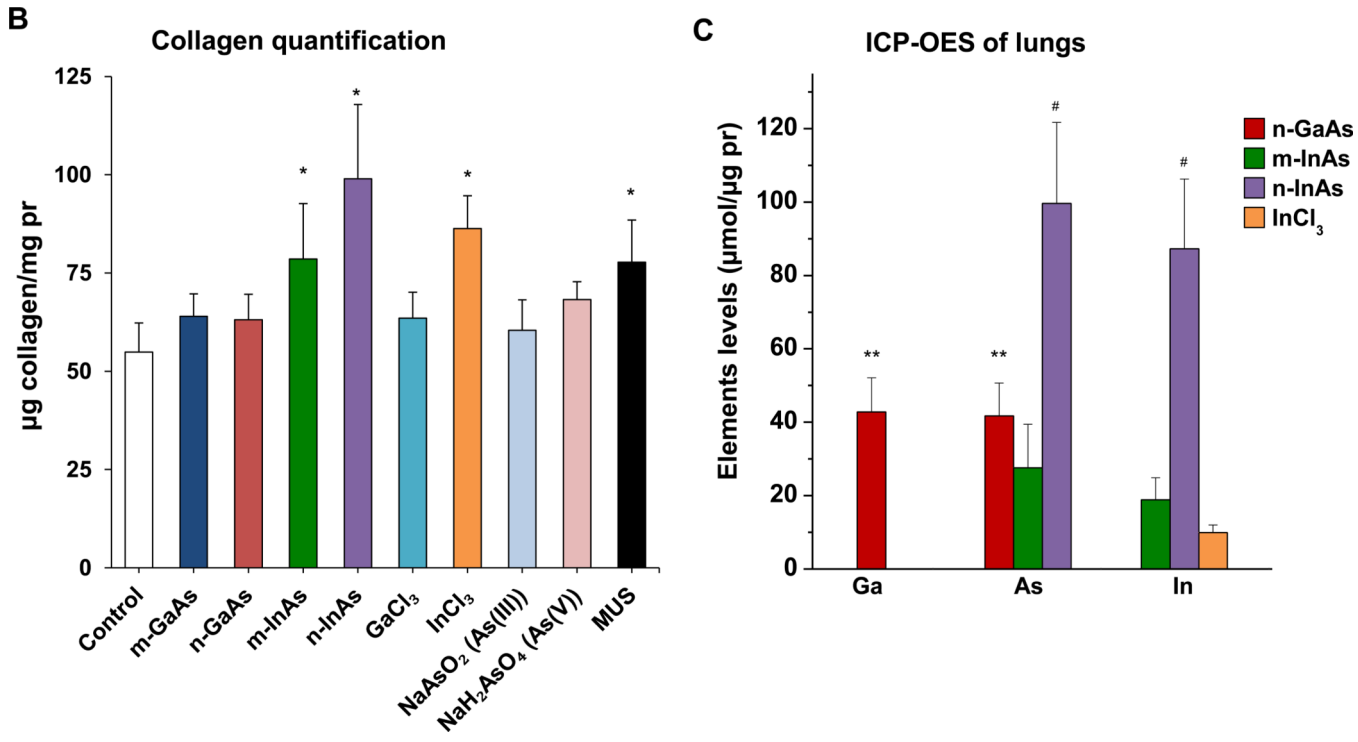

Figure 7.

Pro-fibrogenic effects and elemental analysis, 21 D after initial exposure to particulate and ionic III-V materials. (A) Visualization of collagen deposition (blue-color staining) in the lung by Masson's trichrome staining (100× magnification). MUS served as a positive control. (B) Assessment of total collagen content by using a Sircol kit (Biocolor Ltd., Carrickfergus, UK). (*) $p < 0.05$ compared to control. (C) Elemental Ga, As and In content of the lung by ICP-OES, normalized for protein content in the lung tissue. The intact lungs were collected and processed for ICP-OES analysis as similar as Figure 4. None of the above III-V elements were detected in lung tissue 21 D after m-GaAs, $GaCl_3$, As(III) and As(V) exposure. (**) $p < 0.05$ compared to m-GaAs. (#) $p < 0.05$ compared to m-InAs.

Table 1

Hydrodynamic size (nm) of III-V particles in different aqueous media.

Medium	m-GaAs	n-GaAs	m-InAs	n-InAs
WATER	465.6 ± 9.2	450.8 ± 13.5	317.4 ± 24	213.7 ± 5.3
PBS	1018.9 ± 115.3	358.1 ± 84.3	735.8 ± 416.9	365.5 ± 147.4
RPMI 1640	695.2 ± 13.8	402.4 ± 8.2	408.7 ± 5.9	267.5 ± 7.1
BEGM	761.3 ± 15.4	545.5 ± 12.1	493.8 ± 29.7	343.7 ± 9.9
SBALF	864.7± 65.7	251.7 ± 3.3	369.3 ± 16.9	251.4 ± 111.1
Gamble's solution	1243.2 ± 257.9	561.1 ± 10.4	1078.5 ± 49.6	633.7 ± 365.0

Table 2

Zeta potential (mV) of III-V particles in different aqueous media.

Medium	m-GaAs	n-GaAs	m-InAs	n-InAs
Water	−17.8 ± 1.3	−14.3 ± 2.2	−24.56 ± 1.88	−4.3 ± 2.6
PBS	−16.51 ± 6.4	−14.23 ± 1.3	−29.12 ± 7.18	−8.5 ± 2.0
RPMI 1640	−11.48 ± 2.7	−8.04 ± 1.1	−11.23 ± 5.57	−14.4 ± 2.9
BEGM	−14.38 ± 3.2	−9.73 ± 1.0	−8.38 ± 1.62	−6.3 ± 3.8
sBALF	−8.97 ± 13.4	−11.51 ± 1.0	−14.26 ± 3.61	−15.9 ± 10.2
Gamble’s solution	−8.32 ± 2.91	−7.29 ± 2.45	−8.38 ± 3.40	−3.33 ± 3.08

Table 3

Molar dose and mass dose conversion of III-V materials used *in vitro* and *in vivo*.

Materials	Molar weight (g/mol)	*In vitro*[a]		*In vivo*[b]	
		Molar dose (μmol/mL)	Mass dose (μg/mL)	Molar dose (mmol/kg)	Mass dose (mg/kg)
m-GaAs	144.65	0.043~0.7	6.25~100	0.014	2
n-GaAs	144.65	0.043~0.7	6.25~100	0.014	2
m-InAs	189.74	0.043~0.7	8.15~132.82	0.014	2.62
n-InAs	189.74	0.043~0.7	8.15~132.82	0.014	2.62
$GaCl_3$	176.07	0.043~0.7	7.57~123.25	0.014	2.43
$InCl_3$	221.18	0.043~0.7	9.51~154.82	0.014	3.06
$NaAsO_2$ (AsIII)	129.91	0.043~0.7	5.59~90.94	0.014	1.80
$NaH_2AsO_4{\cdot}7H_2O$ (AsV)	290.03	0.043~0.7	12.47~203.02	0.014	4.01
ZnO (positive control)	81.38	0.043~0.7	3.50~56.97	0.014	1.14
MUS (positive control)	60.08	0.7	42.06	0.083	5

[a] *In vitro* study was performed in THP-1 and BEAS-2B cells.

[b] *In vivo* study was performed in mice at 40 h and 21 D exposure

ACS Nano. Author manuscript; available in PMC 2018 February 28.

Table 4

The effect of n-GaAs on the cytokines production in THP-1 cells by using Cytokine Array.[a]

No.	Cytokines	Dose 0.043 μmol/mL[b]	Dose 0.174 μmol/mL[b]
1	Chitinase 3-like 1	→	↓
2	Complement Factor D	→	↓
3	EMMPRIN	↑	↑
4	GDF-15	→	↓
5	IL-1ra	→	→
6	IL-8	→	→
7	IL-17A	↓	N/A
8	IP-10	↓	N/A
9	MCP-1	↓	↓
10	MIF	↑	↑
11	MIP-1a/MIP-1b	→	↑
12	MIP-3a	↓	↓
13	MMP-9	→	↓
14	Osteopontin	→	↓
15	PDGF-AA	↓	→
16	RANTES	→	↓
17	Serpin E1	→	→
18	uPAR	→	→

[a]THP-1 cells were incubated with n-GaAs NPs at 0.043 and 0.173 μ mol/mL (=6.25 and 25 μg/mL) for 24 h. The supernatant was collected for cytokines and proteins analysis by using Proteome Profiler™ Human XL Cytokine Array Kit. Only 18 were detected among 102 cytokines and proteins (Table S1).

[b]The up- (↑) and down-arrows (↓) indicate an increase or decrease in cytokine levels, while the horizontal arrow (→) indicates no change.

Table 5

Dosimetry Calculations for GaAs in the workplace.[a]

1. GaAs exposure calculation premised on detecting As concentration of 2.7 mg/m^3 in the workplace

$$\frac{2.7(\mathrm{mg\ \ As})}{\mathrm{m}^3}\times\frac{144.645(\mathrm{g\ \ GaAs/mol})}{74.92(\mathrm{g\ \ As/mol})}=5.2(\mathrm{mg\ \ Ga\ \ As})/\mathrm{m}^3$$

2. Calculated weekly nanoparticles lung deposition (mass) in a worker exposed to 5.2 [mg/m] GaAs

Assumptions:

· Ventilation rate of a healthy human adult: 20 [L/min]

· Deposition fraction: 30%

· Weekly exposure period: 8 [h/day], 5 [d/week]

Weekly lung deposition:

$$\frac{5.2\mathrm{mg}}{\mathrm{m}^3}\times\frac{20\mathrm{L}}{\mathrm{min}\cdot\mathrm{person}}\times 30\%\times\frac{60\mathrm{min}}{\mathrm{hour}}\times\frac{8\mathrm{hour}}{\mathrm{day}}\times\frac{5\mathrm{day}}{\mathrm{week}}\times\frac{\mathrm{m}^3}{1000\mathrm{L}}=74.88\mathrm{mg}$$

3. Weekly deposition level converted to mass/surface area in the human lung

Assumptions:

· Human alveolar surface area: 102 [m /person]

Calculation:

$$\frac{74.88\mathrm{mg}}{\mathrm{person}\cdot\mathrm{week}}\times\frac{\mathrm{person}}{102\mathrm{m}^2}=\frac{1000\mu\mathrm{g}}{\mathrm{mg}}=734.12\mu\mathrm{g}/\mathrm{m}^2$$

4. Comparable deposition level in a mouse receiving a one-time installation exposure

Assumptions:

· Alveolar epithelium surface area of a mouse: 0.05 [m /mouse];

· Weight of a mouse: 25 [g]

Calculation:

$$\frac{734.12\mu\mathrm{g}}{\mathrm{m}^2\cdot\mathrm{week}}\times\frac{0.05\mathrm{m}^2}{\mathrm{mouse}}\times\frac{1\mathrm{mg}}{1000\mu\mathrm{g}}\times\frac{\mathrm{mouse}}{25\mathrm{g}}\times\frac{1000\mathrm{g}}{\mathrm{kg}}=1.468\mathrm{mg/kg}$$

[a] Our animal experiments were based on a real-life As exposure measurement in a manufacturing facility, where airborne As levels were documented to be as high as 2.7 mg/m^3.[34] The chosen dose of 0.014 mmol/kg for each of the III-V materials equals to 1–4 mg/kg based on the molar weight in Table 3, which overlaps with the calculated mouse exposure dose of 1.468 [mg/kg].